Wwc2 is a novel cell division regulator during preimplantation mouse embryo lineage formation and oogenesis

Giorgio Virnicchi[1*], Pablo Bora[1], Lenka Gahurová[1], Andrej Šušor[2] and Alexander W. Bruce[1*]

[1] Laboratory of Early Mammalian Developmental Biology (LEMDB),
Department of Molecular Biology & Genetics,
Faculty of Science,
University of South Bohemia,
Branišovská 31,
370 05 České Budějovice (Budweis),
CZECH REPUBLIC.

[2] Laboratory of Biochemistry and Molecular Biology of Germ Cells,
Institute of Animal Physiology and Genetics,
Czech Academy of Sciences, Rumburská 89,
277 21 Liběchov,
CZECH REPUBLIC.

[*]correspondence; A.W.B. awbruce@prf.jcu.cz & G.V. giorgio.virnicchi@gmail.com
Tel: +420387772291
Fax: +42038777226 (not confidential)

Manuscript length (body text): 7818 words
Number of figures: 8

Running title: *Wwc2*: early developmental cell-division regulator

ABSTRACT

Formation of a mature and hatching mouse blastocyst marks the end of the preimplantation development, whereby regulated cell cleavages culminate in the formation of three distinct lineages. We report dysregulated expression of *Wwc2*, an ill-characterised paralog of the Hippo-signalling activator *Kibra/Wwc1*, is specifically associated with cell autonomous deficits in embryo cell number and cell division abnormalities, typified by imbalanced daughter cell chromatin segregation. Division phenotypes are also observed during mouse oocyte meiotic maturation, as *Wwc2* dysregulation blocks progression to the fertilisation competent stage of meiosis II metaphase arrest, characterised by spindle defects and failed Aurora-A kinase (AURKA) activation. Such cell division defects, each occurring in the absence of centrosomes, are fully reversible by expression of recombinant HA-epitope tagged WWC2, restoring activated oocyte AURKA levels. Additionally, clonal dysregulation implicates *Wwc2* in maintaining the pluripotent late blastocyst stage epiblast lineage. Thus, *Wwc2* is a novel regulator of meiotic and early mitotic cell divisions, and mouse blastocyst cell-fate.

INTRODUCTION

Following the fertilisation of mouse metaphase II arrested secondary (MII) oocytes, a series of asynchronous cleavage divisions generates blastocysts comprising three distinct cell lineages: an outer-residing, differentiating and apical-basolaterally polarised epithelium called the trophectoderm (TE, a progenitor of placental tissue), a further polarised mono-layer of differentiating inner-cell mass (ICM) cells in contact with the fluid filled cavity comprising the primitive endoderm (PrE, progenitors of yolk sac membranes) and pluripotent cells completely encapsulated in the ICM known as the epiblast (EPI, foetal cell progenitors) (see reviews - Frum and Ralston, 2015;Chazaud and Yamanaka, 2016;Rossant, 2016;Mihajlovic and Bruce, 2017;Rossant, 2018;White et al., 2018). Differential regulation of Hippo-signalling (originally identified in *Drosophila* as a cell proliferation and tissue growth regulating pathway, now implicated in varied developmental/pathological paradigms (Davis and Tapon, 2019)) has been identified as an important mechanism of blastocyst lineage specification. Without listing all involved molecular players (see reviews (Hirate et al., 2015;Chazaud and Yamanaka, 2016;Sasaki, 2017)), polarity dependent Hippo-pathway suppression in outer cells enables formation of activating TEAD4 transcriptional complexes (involving nuclear localisation of specific co-factors, YAP and WWTR1/TAZ, collectively referred to here as YAP) to potentiate TE specific gene expression, whereas activated Hippo-signalling in apolar inner cells inhibits this process (via activating LATS1/2 kinases to prevent YAP nuclear localisation)(Nishioka et al., 2009). TEAD4-YAP complexes also simultaneously suppress pluripotent gene expression (*e.g. Sox2*) in derived outer-cells (Wicklow et al., 2014;Frum et al., 2018) and prevent precocious *Sox2* expression prior to the 16-cell stage (Frum et al., 2019). However, eventual EPI specification by the late blastocyst stage, actually requires ICM cell YAP redistribution to the nucleus (implying suppression of Hippo-signalling); an inherently heterogeneous process causing competitive apoptotic elimination of EPI progenitors of reduced naïve pluripotency (Hashimoto and Sasaki, 2019). Collectively, these data illustrate the important and integral nature of Hippo-signalling in regulating key cell-fate events in early mouse embryogenesis and suggests roles for other, particularly upstream and potentially novel, factors capable of functionally interacting with core Hippo-pathway machinery.

The *Drosophila* WW-domain and C2-domain containing (WWC-domain) gene *Kibra* is a positive regulator of Hippo-signalling, causing phosphorylation of the fly orthologue of mammalian LATS1/2 (warts/Wts) in tumour suppressor screens (Baumgartner et al., 2010;Genevet et al., 2010;Yu et al., 2010); a role subsequently confirmed in mammalian cell lines (Xiao et al., 2011a). Unlike *Drosophila*, tetrapod genomes typically encode three WWC-domain paralogs, called *KIBRA/WWC1*, *WWC2* and *WWC3*, although the *Mus musculus* genome does not contain a *Wwc3* gene due to an evolutionarily recent chromosomal deletion. The paralogous human WWC-domain proteins are highly conserved, cable of homo- and hetero-dimerisation, can all activate Hippo-signalling (causing LATS1/2 and YAP phosphorylation) and cause the Hippo-related *Drosophila* 'rough-eye' phenotype, caused by reduced cell proliferation, when over-expressed in the developing fly eye (Wennmann et al., 2014). Despite a comparatively large and pan-model KIBRA-related literature, the roles of WWC2/3 are considerably understudied and restricted to limited prognostic reports consistent of tumour suppressor function in specific cancers (*e.g.* hepatocellular carcinoma (Zhang et al., 2017) and epithelial-mesenchymal lung cancers (Han et al., 2018)). There are no reports of any functional roles for WWC-domain containing genes during mammalian preimplantation development.

Ovulated mouse MII oocytes arise from the maturation of subpopulations of meiosis I (MI) prophase arrested primary oocytes, stimulated to re-enter meiosis by maternal reproductive hormones (reviewed (Sanders and Jones, 2018)). Meiotic resumption ensures necessary growth required to support later embryonic development and expression of gene products required to execute meiosis; faithfully segregate homologous chromosome bivalents, form the first polar body and a developmentally competent MII oocyte (itself capable of correctly segregating sister chromatids post-fertilisation). Failed chromosome segregation, resulting in egg and/or zygotic aneuploidy, has usually terminal consequences for embryonic development and aneuploidy attributable to the human female germline is recorded as the leading single cause of spontaneously aborted pregnancy (Hassold and Hunt, 2001;Nagaoka et al., 2012). An extensive literature covering many aspects of the germane segregation of homologous chromosomes during MI exists (see comprehensive reviews (Bennabi et al., 2016;Mihajlovic and FitzHarris, 2018;Mogessie et al., 2018;Namgoong and Kim, 2018;Sanders and Jones, 2018)). As in all mammals, and unlike most mitotic somatic cells, mouse meiotic spindle formation occurs in the absence of centrioles/centrosomes and is initiated around condensed chromosomes from coalescing microtubule organising centres (MTOCs) that are further stabilised by chromosome derived RAN-GTP gradients (Bennabi et al., 2016;Severson et al., 2016;Gruss, 2018;Mogessie et al., 2018;Namgoong and Kim, 2018). Transition from MTOC initiated spindle formation to centrosomal control in mice only occurs by the mid-blastocysts (E4.0) stage, when centrosomes appear *de novo* ((Courtois et al., 2012)). This contrasts with other mammals were fertilising sperm provide a founder centriole that duplicates and ensures the first mitotic spindle is assembled centrosomally (Sathananthan et al., 1991;Schatten and Sun, 2009). Amongst known key regulators of meiotic/mitotic spindle dynamics are the conserved Aurora-kinase family (AURKA, AURKB & AURKC, collectively referred to here as AURKs) that all exhibit germ cell and early embryonic expression (AURKC is not expressed in other somatic cells (Li et al., 2017)). During meiosis, AURKs have important regulatory roles during spindle formation/organisation, MTOC clustering, chromosome condensation and alignment. Moreover, in mitosis, AURKs regulate correct microtubule-kinetochore attachment, chromosomal cohesion and cytokinesis (reviewed in (Nguyen and Schindler, 2017)). Specifically, AURKA protein is essential for MI progression (Saskova et al., 2008) and continually localises with MTOCs and MI/MII spindle poles, regulating MTOC clustering and initiating microtubule nucleation/dynamics, throughout oocyte meiosis (Swain et al., 2008;Solc et al., 2012;Nguyen and Schindler, 2017;Nguyen et al., 2018); with similar roles in post-fertilisation zygotes (Kovarikova et al., 2016).

We report abrogated *Wwc2* expression in mouse embryo blastomeres causes cell autonomous cleavage division phenotypes, yielding blastocysts with fewer overall cells, mis-segregated chromosomes and defective cytokinesis (not replicated by targeted *Kibra* expression). Cell division phenotypes in meiotically maturating mouse oocytes are also caused by RNAi targeted *Wwc2* expression and are coincident with spindle defects and blocked activation of AURKA. Such phenotypes are rescuable by expression of epitope-tagged recombinant WWC2 protein, that in embryos localises with mid-body structures and restores appropriate cellular contribution to the pluripotent EPI, normally lacking after *Wwc2* dysregulation.

MATERIALS & METHODS

Mouse embryo related experimental procedures were approved and licensed by local ethics committees at the Biology Centre (in České Budějovice) of the Czech Academy of Sciences in accordance with Act No 246/1992

130 for the protection of animals against cruelty; issued by Ministry of Agriculture of the Czech Republic, 25.09.2014,
131 number CZ02389.
132
133 **Embryo and oocyte culture and microinjection.**
134 2-cell stage (E1.5) embryo collection, from super-ovulated and mated 10 week old F1 hybrid (C57Bl6 x
135 CBA/W) female mice, and *in vitro* culture in mineral oil covered drops (~20 µL/ ~15 embryos) of commercial KSOM
136 (EmbryoMax® KSOM without Phenol Red; Merck, MR-020P-5F), conducted as previously described (Mihajlovic
137 et al., 2015). Germinal vesicle (GV) stage primary oocytes were mechanically recovered into M2 media (containing
138 100 µM 3-isobutyl-1-methylxanthine/IBMX; cAMP/cGMP phosphodiesterase inhibitor that maintains GV meiosis I
139 arrest)) from mature Graafian follicles of dissected ovaries of dams after PMSG (pregnant mare serum
140 gonadotrophin) hormone stimulation (7.5U intraperitoneal injection of F1 hybrid strain, 48 hours prior). Recovered
141 oocytes placed into pre-warmed (37°C) drops (~20 µl/ ~15 oocytes) of commercial CZB media (EmbryoMax® CZB
142 media with Phenol Red; Merck, MR-019-D; +IBMX) , overlaid with mineral oil and incubated (37°C/ 5% CO_2) for
143 2 hours prior to microinjection.
144 Individual blastomere dsRNA, siRNA or recombinant mRNA microinjections (or combinations thereof), plus
145 post-microinjection culture protocols, performed on 2-cell stage embryos (in either one or both blastomeres)
146 according to defined protocols (Zernicka-Goetz et al., 1996), using apparatus formerly described (Mihajlovic et al.,
147 2015). Recovered GV staged oocytes microinjected using a minimally adapted protocol; namely oocytes were
148 microinjected on 37°C heated stage in concaved glass microscope slides filled with CZB media (+100 µM IBMX),
149 overlaid with mineral oil. Post-microinjection, GV oocytes returned to the incubator for another 18 hours (to permit
150 microinjected siRNA mediated gene knockdown or mRNA expression; CZB +IBMX media) then transferred to pre-
151 equilibrated CZB media drops lacking IBMX, to induce resumption of meiosis I and *in vitro* maturation (IVM).
152 Cultured (and microinjected) embryos/oocytes assayed at various developmental points, as dictated by individual
153 experiments. As indicated, rhodamine-conjugated dextran beads (RDBs; 1 µg/ µl – ThermoFisher Scientific, D1818)
154 were co-microinjected to confirm successful blastomere/oocyte microinjection; a summary of the origin and
155 concentrations of all microinjected RNA species is given in supplementary methods tables SM1. Non-microinjected
156 embryos, or oocytes, (2-3 per microinjection experiment, per plate) served as culture sentinels to confirm successful
157 *in vitro* embryo development/oocyte maturation. In cases of AURKA chemical inhibition (to confirm specificity of
158 anti-p-AURKA antisera), recovered GV oocytes were transferred from IMBX containing CZB media to pre-
159 equilibrated CZB drops lacking IBMX but containing specific AURKA inhibitor, MLN8237 (1µM; Selleckchem,
160 S1133).
161
162 **dsRNA and recombinant mRNA synthesis.**
163 Specific long dsRNA molecules targeting coding regions of mouse *Kibra* and *Wwc2* derived transcripts
164 (plus negative control GFP) were designed (and *in silico* validated using online E-RNAi resource (Horn and Boutros,
165 2010)) and synthesised. Briefly, gene specific PCR primer pairs, incorporating 5'- T7-derived RNA polymerase
166 promoters and spanning designed dsRNA complementary sequence, were used to derive *in vitro* transcription (IVT)
167 template, using mouse blastocyst (E3.5) cDNA as a template (or plasmid DNA for GFP). After agarose gel
168 verification, double stranded DNA templates were used in preparatory IVM reactions, incorporating DNaseI and

169 single-stranded RNase treatment (MEGAscript T7; ThermoFisher Scientific, AMB13345), generating dsRNA. The
170 integrity of derived *Kibra*-, *Wwc2*- and *GFP*-dsRNAs was confirmed by non-denaturing gel electrophoresis and
171 quantified (Nanodrop). PCR primer sequences used are provided in supplementary methods table SM2.
172 Microinjected mRNA constructs derived using commercially available IVT reaction kit (mMACHINE T3;
173 ThermoFisher Scientific, AM1348), using restriction enzyme linearized (using *SfiI*) plasmid DNA as template (2 µg)
174 as follows; i. C-terminal GFP-fusion *Gap43* mRNA plasma membrane marker, from pRN3P-C-term-GFP-Gap43
175 (Morris et al., 2010)), ii. C-terminal RFP-fusion histone H2B mRNA (from pRN3-C-term-RFP-Hist1h2bb, derived
176 in this study) and iii. siRNA-resistant N-terminal HA-tagged *Wwc2* mRNA (from pRN3P-N-term-HA-siRNAres-
177 Wwc2, derived here). All synthesised mRNAs subject to post-synthesis 3' poly-adenylation (Poly(A) Tailing Kit -
178 ThermoFisher Scientific, AM1350), confirmed by denaturing gel electrophoresis and quantified (Nanodrop).
179
180 **Recombinant plasmid construct generation.**
181 Four recombinant plasmids (required for IVT) generated using standard molecular biological protocols.
182 RFP-histone H2B fusion protein (pRN3-C-term-RFP-Hist1h2bb) derived by in frame cloning of a high-fidelity PCR
183 amplified cDNA (Phusion® DNA polymerase, New England BioLabs, M05305) encoding histone H2B (*Hist1h2bb,*
184 lacking endogenous start and stop codons), flanked by oligonucleotide introduced restriction sites (*NheI*), into RNA
185 transcription cassette plasmid pRN3-insert-RFP variant (vector encodes required start and stop codons). Thus,
186 generating required H2B-RFP fusion reporter, downstream of vector encoded T3 RNA polymerase promoter (for
187 IVT) and flanked by UTRs from the frog β-globin gene (Lemaire et al., 1995). The IVT plasmid encoding the siRNA-
188 resistant N-terminal HA-tagged *Wwc2* mRNA (pRN3P-N-term-HA-siRNAres-Wwc2) was created from an annotated
189 full-length Riken mouse *Wwc2* cDNA clone (clone ID: M5C1098O04, Source Bioscience) by deriving high fidelity
190 PCR product, with oligo introduced 5' (*SpeI*) and 3' (*NotI*) restriction sites and an in frame N-terminal HA-epitope
191 tag, and 'TA cloned' (after addition of 3' adenine nucleotide overhangs) it into pGEM®-T-Easy plasmid vector
192 (Promega, A1360). The derived plasmid was mutagenised (commercial service; EuroFins) to alter nucleotide (but
193 not redundant amino acid codon) sequence of the siRNA (utilised in this study) recognition motif. The recombinant
194 gene sequence was sub-cloned, using introduced *SpeI* and *NotI* restriction sites, into the multiple cloning site of the
195 RNA transcription cassette plasmid pRN3P (Zernicka-Goetz et al., 1996) to derive IVT competent pRN3P-N-term-
196 HA-siRNAres-Wwc2. All four derived plasmids were sequence verified and the PCR primers (or relevant details)
197 used to generate the required inserts are described in supplementary methods table SM3.
198
199 **Q-RT-PCR**
200 Per experimental condition, total RNA was extracted from ~30 (microinjected) mouse embryos (oocytes) *in*
201 *vitro* cultured to the desired developmental stage, using PicoPure RNA isolation kit (Arcturus Biosciences/
202 ThermoFisher Scientific, KIT0204), as instructed. Eluted RNA (10 µL) was DNaseI treated (DNA-*free* kit;
203 ThermoFisher Scientific, AM1906) and used to derive cDNA (30 µL), either via oligo-dT (embryos and oocyte) or
204 random hexamer (oocytes only) priming (Superscript-III Reverse Transcriptase; ThermoFisher Scientific,
205 18080085). 0.5 µl of diluted template cDNA (1:3, nuclease-free water) per real-time PCR reaction (10 µl – SYBR
206 Green PCR kit, Qiagen, 204143) was used to assay specific transcript abundance (CFX96 Real-Time System,
207 BioRad). *Kibra* and *Wwc2* transcript levels were internally normalised against those for *Tbp* (TATA-binding protein)

208 housekeeping gene and fold changes (±s.e.m.) derived using the ΔΔCt method (Livak and Schmittgen, 2001). A
209 minimum of two biological replicates of at least three technical replicates were employed; specific gene oligo primer
210 sequences (final reaction conc. 400 nM) are in supplementary methods table SM4.
211
212 **Immuno-fluorescent staining and confocal microscopy imaging**.
213 *In vitro* cultured (microinjected) embryos/oocytes were fixed (at required developmental stages) with 4%
214 para-formaldehyde, immuno-fluorescently (IF) stained and imaged in complete z-series by confocal microscopy
215 (using FV10i confocal microscope, Olympus) as described (Mihajlovic et al., 2015); supplementary methods table
216 SM5 summarises the identity and combinations (plus employed concentrations) of primary and fluorescently
217 conjugated secondary antibodies used. The majority of IF stained embryos/oocytes were counterstained for DNA,
218 using DAPI containing mounting solution (Vectashield plus DAPI, Vector Labs) and as indicated some embryo
219 samples were also counterstained against filamentous-actin, using fluorescently-labelled rhodamine-conjugated
220 phalloidin (ThermoFisher, R415 - described in (Mihajlovic and Bruce, 2016)).
221
222 **Embryo/oocyte image analysis/ cell counting.**
223 Contributions of each individual cell, per fixed embryo sample (in control or *Kibra/Wwc2* gene RNAi KD
224 conditions), to; inner (entirely encapsulated) outer (whereby cells retain cell contactless domains) embryo
225 compartments, emerging blastocyst cell lineages (defined by presence and/or absence of specific and stated lineage
226 marker protein expression), cell populations defined by presence of a defining intra-cellular feature (*e.g.* cell/nuclei
227 morphological abnormalities, apoptosis, lineage marker protein or mid-bodies) or presence within or outwith a
228 microinjected clone (distinguishable by a fluorescent injection marker signal, *i.e.* RDBs or recombinant fluorescent
229 fusion proteins) was determined by serial inspection of individual confocal micrograph z-sections of each embryo,
230 using commercial Fluoview ver.1.7.a (Olympus), Imaris (Bitplane) and ImageJ software. These calculated
231 contributions were individually tabulated (see supplementary tables) and the mean of cells within defined sub-
232 populations, plus standard error of means (mean ± s.e.m.) determined. The statistical significance between relevant
233 experimental and control groups was determined using 2-tailed Student's t-tests (experiment specific supplementary
234 tables provide comprehensive summaries, plus all individual embryo data). Relating to oocytes, a similar approach
235 was used to assay mean frequencies by which maturing oocytes exhibit intra-cellular morphologies (revealed by
236 combined IF staining - *i.e.* α-TUBULIN and p-AURKA and microinjected fluorescent reporter protein expression -
237 *i.e.* RFP-histone H2B) indicative of appropriate or aberrant oocyte maturation (as categorised), at the indicated
238 developmental time-point; such data are summarised in relevant supplementary tables, including individual oocyte
239 derived data.
240
241 **Western blotting**
242 Precise numbers of oocytes per comparable experimental condition (~15-30) were washed in phosphate
243 buffer saline (PBS; Merck, P5493) containing polyvinyl alcohol (PVA; Merck, 341584), frozen in a residual volume
244 at -80°C, before lysis, in 10 µl of 10x SDS reducing agent/loading buffer (NuPAGE buffer, ThermoFisher Scientific,
245 NP 0004, ThermoFisher Scientific), by boiling at 100°C for 5 minutes. Loaded proteins were electrophoretically
246 separated on gradient precast 4–12% SDS–PAGE gels (ThermoFisher Scientific, NP0323) and transferred to

247 Immobilon P membranes (Merck group, IVPD00010) using a semi-dry blotting system (Biometra/ Analytik Jena)
248 for 25 minutes at 5 mA/cm^2. Blotted membranes were blocked in 5% skimmed milk powder dissolved in 0.05%
249 Tween-Tris pH 7.4 buffered saline (TTBS) for 1 hour, briefly rinsed in TTBS and then incubated overnight at 4°C in
250 1% milk/TTBS containing primary antibody. Membranes were washed in three changes of TTBS buffer (20 minutes
251 each at room temperature) and horse-radish peroxidase conjugated secondary antibody added to the blot in 1%
252 milk/TTBS, for 1 hour (room temperature). Immuno-detected proteins were visualized by chemiluminescent
253 photographic film exposure (ECL kit; GE Life Sciences, RPN2232) and digitally scanned using a GS-800 calibrated
254 densitometer (Bio-Rad Laboratories). Antibody stripped membrane blots were re-probed, for loading controls, in an
255 identical manner. Supplementary methods tables SM6 details the utilised concentrations of the primary and
256 peroxidase-conjugated secondary antibodies used.
257
258 **Supplementary materials**
259 Three components: a) Supplementary Figures S1- S10, plus legends, b) Supplementary Methods Tables SM1
260 – SM6 and c) Supplementary Tables ST1 – ST26 (detailing all analysed embryo/oocyte cell counts and statistics).
261
262 **RESULTS**
263
264 **WWC-domain gene expression in preimplantation mouse embryos**
265 In the central context of Hippo-signalling during early mouse development (Sasaki, 2017), we investigated
266 the potential role of WWC-domain containing genes (*Kibra* and *Wwc2* (Wennmann et al., 2014)) during blastocyst
267 formation. We assayed *Kibra* and *Wwc2* mRNA expression levels after microinjection of control dsRNA or constructs
268 specific for each gene (Fig. 1a). Stable levels of *Kibra* and *Wwc2* transcripts were readily detectable at both 8- (E2.5)
269 and 32-cell (E3.5) stages, with normalised *Wwc2* expression twice as abundant as *Kibra*. Each transcript could be
270 robustly depleted using dsRNA mediated global knockdown (KD) at both assayed stages, although we could not
271 assay protein expression due to a lack of reliable anti-sera. We next assayed for overt developmental defects
272 associated with individual or combined *Kibra*/*Wwc2* KD by microinjecting dsRNA(s) in one blastomere of 2-cell
273 (E1.5) stage embryos, culturing to the late blastocyst (E4.5) stage and counting total cell number (Fig. 1b). *Kibra*
274 gene KD had no significant effect on total cell number (versus control dsRNA) but a severe attenuation when targeting
275 *Kibra* and *Wwc2* transcripts together was observed. This defect was statistically indistinguishable from embryo
276 groups microinjected with *Wwc2* dsRNA alone, indicating sole *Wwc2* KD was sufficient to induce the observed
277 phenotype (note, *Kibra* mRNA levels were unaffected by *Wwc2* dsRNA at the 8-cell stage, whereas *Wwc2* transcripts
278 were robustly reduced, confirming *Wwc2* dsRNA specificity – Fig. 1a and supplementary Fig. S1). Repetition of
279 *Wwc2* KD, in a fluorescently marked clone (rhodamine conjugated dextran beads/ RDBs were co-microinjected with
280 *Wwc2* dsRNA) confirmed reduced cell numbers, as early as the 16-cell (E3.0) stage, specifically within the marked
281 clone that itself had reduced contribution to the initial inner-cell/ICM founding population (Fig. 1c). Accordingly,
282 we focussed further investigations on the overt cell number deficit caused by *Wwc2* KD.
283
284 **Reduced embryo cell numbers caused by *Wwc2* KD are associated with defective cell division.**

285 Although the utilised *Wwc2* dsRNA was carefully designed to avoid off target effects (specifically relating
286 to *Kibra* expression, Figs. 1a & S1), we sought to make a phenocopy using an siRNA mediated approach (targeting
287 an alternative *Wwc2* mRNA region – Fig. S1). In addition to confirming the phenotype, the switch was adopted to
288 permit phenotypic rescue experiments, by expressing recombinant siRNA-resistant *Wwc2* mRNA (see below). The
289 *Wwc2* siRNA near completely eliminated detectable *Wwc2* transcripts in global KD (Fig. 2b). A subsequent assay of
290 total cell number at all cleavage stages, revealed an accumulative and statistically robust deficit beginning after the
291 8-cell stage (Fig. 2c). Indeed, from the equivalent 8- to 32-cell stages (relative to control embryo development), total
292 cell number did not significantly increase in *Wwc2* KD embryos but did start to increase during the blastocyst
293 maturation period (32- to >64-cell stages). Next, we assayed if *Wwc2* siRNA phenotypes were cell autonomous by
294 creating RDB marked *Wwc2* specific siRNA KD clones (comprising 50% of the embryo – Fig. S2). We observed a
295 statistically significant *Wwc2* siRNA mediated deficit in cell number within the microinjected clone (versus both the
296 non-microinjected sister clones and the equivalent microinjected clones in control siRNA embryos), at all post-8-cell
297 stages. We did not observe significant differences between control and *Wwc2* KD groups in the number of cells within
298 the non-microinjected clone (with the exception of the 32-cell stage where there was an average of 2.3 fewer cells in
299 the *Wwc2* KD group). These data support a novel and cell autonomous role for *Wwc2* in ensuring appropriate cell
300 number during preimplantation mouse embryo development.
301 We also observed a number of morphological nuclear abnormalities within *Wwc2* KD embryos and cell
302 clones, not evident in the controls. Illustrative examples, at the 32-cell equivalent stage are provided (Fig. 3b) and
303 were categorised as; 'abnormal nuclear morphology' (including that typical of 'association with the mid-body'),
304 associated with 'cytokinesis defects' (typified by bi-nucleated cells) or coincident with 'multiple or micronuclei'.
305 We calculated the frequencies by which each or a composite of such abnormalities were observed at each assayed
306 cleavage stage; defined per embryo (in at least one blastomere) or per individual assayed cell (Fig. 3c). Apart from a
307 single incidence of an early blastocyst stage cell exhibiting a single micronucleus, no abnormalities were observed
308 in any control siRNA microinjected embryo, at any developmental stage. Conversely, at the 8-cell stage abnormally
309 shaped nuclei were present in over a quarter of *Wwc2* global KD embryos and in all assayed embryos by the
310 equivalent late blastocyst stage. A similar trend assaying multiple/micronuclei was observed from the 16-cell stage.
311 Although less prevalent, cytokinetic defects also affected nearly a quarter of *Wwc2* KD embryos at the late blastocyst
312 stage. Indeed, all *Wwc2* global KD embryos exhibited one or more defect, in at least one cell, by the mid-blastocyst
313 stage, with the collective defects (excluding cytokinesis/bi-nucleation) first arising in just over a quarter of 8-cell
314 stage embryos. An assay of the same phenotypes at the level of each individually assayed blastomere showed that
315 just over a quarter of cells were affected by the late blastocyst stage, although such embryos comprised a much
316 smaller average of overall cells, versus control siRNA groups (*i.e.* 31.3±3.0 against 87.0±3.8 - Fig. 2c). Thus,
317 cleavage stage *Wwc2* KD is associated with cell autonomous division defects that contribute to embryos with
318 progressively fewer constituent blastomeres from the 8-cell stage and invokes a role for *Wwc2* in regulating
319 appropriate cell division in the early mouse embryo.
320
321 ***Wwc2* mRNA depletion in primary (GV) oocytes impairs meiotic maturation.**
322 We next addressed whether similar *Wwc2* KD in germinal vesicle (GV) oocytes could cause subsequent
323 meiotic division defects, particularly as both embryo cleavage divisions and meiotic oocyte maturation occur in the

absence of centrosomes in mice (Courtois et al., 2012;Coelho et al., 2013;Bennabi et al., 2016;Severson et al., 2016;Gruss, 2018;Mogessie et al., 2018;Namgoong and Kim, 2018). We first confirmed by Q-RT-PCR abundant *Wwc2* transcript expression in GV and MII oocytes (plus zygotes). Exploiting alternative, oligo-dT versus random hexamer, cDNA synthesis priming strategies we uncovered evidence of cytoplasmic *Wwc2* mRNA poly-adenylation, usually associated with increased translational efficiency of functionally important proteins during meiotic maturation (Salles et al., 1992) - Fig. 4a. Consultation of our previously published assay of polysome associated transcripts during mid meiotic maturation supported this interpretation, reporting ~40% polysome association of detectable *Wwc2* transcripts (Koncicka et al., 2018). We then confirmed our siRNA construct could elicit robust *Wwc2* transcript knockdown in microinjected GV oocytes, that had been blocked from re-entering meiosis I (using a cAMP/cGMP phosphodiesterase inhibitor, 3-isobutyl-1-methylxanthine/ IMBX) and then permitted similarly treated oocytes to *in vitro* mature (IVM) to the MII equivalent stage (Fig. 4b & c). Such oocytes were fixed and immuno-fluorescently (IF) stained for α-Tubulin (plus DAPI DNA stain) and assayed by confocal microscopy for potential meiotic maturation/division phenotypes. In the two control conditions (non-microinjected or control siRNA microinjected oocytes) >90% of GV oocytes matured to the MII arrested stage, typified by extruded polar bodies (PB1) and metaphase II arrested spindles. However, in the *Wwc2* KD group, this successful IVM rate was reduced to 8.6%. The remaining oocytes presented with various MI arrested phenotypes (all lacking PB1) categorised by; presence of MI metaphase spindles (-PB1 +MI spindle; 42.9%, note spindles typically failed to migrate to oocyte cortex), spindle-like structures with mis-aligned or dispersed chromosomes (-PB1 +spindle defect; 22.9%) or non-nuclear membrane enveloped chromatin devoid of associated α-Tubulin (-PB1+ultra-condensed chromatin; 25.7%). Such phenotypes collectively indicate profoundly defective oocyte meiotic maturation and impaired homologous chromosome segregation caused by *Wwc2* KD (Fig. 4d & d'). Although assayed oocytes were subject to IVM for 18 hours, we wanted to exclude the possibly the results were indicative of delayed rather than blocked meiotic progression. Consistently, experimental repetition using an extended IVM period of 24 hours did not reveal any increased frequency of MII arrested oocyte generation. Indeed, *Wwc2* KD oocytes either remained blocked in MI or unsuccessfully attempted chromosome segregation without undergoing cytokinesis (Fig. S3).

***Wwc2* KD oocyte phenotypes are associated with failed Aurora kinase-A (AURKA) activation.**

Phosphorylation dependent activation of Aurora kinase-A (p-AURKA: p-Thr288) is required to initiate acentrosomal and MTOC mediated spindle assembly in mouse oocytes and *Aurka* KD phenotypes closely resemble the *Wwc2* KD defects we describe (Bury et al., 2017). We hypothesised the observed *Wwc2* specific meiotic maturation phenotypes may be associated with impaired p-AURKA activation. Western blot analyses of staged maturing oocytes confirmed characteristically low p-AURKA levels in GV oocytes, that markedly increased in the presence of the MI spindle and were maintained when the MII spindle was formed (Fig. 5b (Saskova et al., 2008;Nguyen and Schindler, 2017)); a trend replicated in control siRNA microinjected GV and resulting MII oocytes (note, anti-p-AURKA antibody specificity was independently confirmed; Fig. S4). However, p-AURKA was not detectable at either the equivalent GV or MII stages in *Wwc2* siRNA microinjected oocytes. Moreover, p-AURKA immuno-reactivity (assayed by confocal microscopy based IF) that would ordinarily localise to spindle poles or spindle-like structures, was also lacking in *Wwc2* KD oocytes. This a stark contrast to that observed on MII arrested spindles in control oocytes (Fig. 5c – note, the p-AURKA channel of the example *Wwc2* KD oocyte is over-exposed

363 to illustrate the lack of spindle associated immuno-reactivity but accentuates non-specific cortical auto-fluorescence
364 also seen in control oocytes). These results confirm failed p-AURKA activation during oocyte maturation, under
365 conditions of experimentally induced *Wwc2* KD, associated with profoundly defective meiotic cell division.
366 Despite consistent *Wwc2*-specifc RNAi cell division phenotypes uncovered with distinct dsRNA/siRNA
367 constructs in preimplantation mouse embryos/oocytes (plus optimised design to avoid potential off-target effects or
368 cross reactivity with paralogous *Kibra* mRNA - Figs. 1 and S1), we sought further verification of the identified *Wwc2*
369 specific oocyte role. Accordingly, we derived a recombinant and N-terminally HA-epitope tagged *Wwc2* mRNA
370 construct (*HA-Wwc2*), specifically mutated within the siRNA complementary sequence (yet preserving, via
371 redundancy, the sequence of amino acid codons; Fig. S5), that could remain available for translation in *Wwc2* siRNA
372 microinjected oocytes. Repeating the described IVM experiments (but assaying at multiple time-points), we found
373 that co-microinjection of *HA-Wwc2* mRNA and *Wwc2* siRNA caused a robust rescue of the maturation phenotypes
374 previously observed by *Wwc2* siRNA microinjection alone (MII arrested oocytes +PB1, 16 hours post-IBMX; control
375 siRNA – 81.8%, *Wwc2* siRNA - 8.7% & *HA-Wwc2* mRNA plus *Wwc2* siRNA – 76.0%). Moreover, the progression
376 of the observed rescue through recognisable oocyte maturation stages was in-step with that of control siRNA
377 microinjected oocytes (as measured at 1, 6, 12 and 16 hours post-IBMX; Fig. 5d). We also found *HA-Wwc2* mRNA
378 co-microinjection was associated with reappearance of detectable p-AURKA protein expression (Fig. 5e), and sub-
379 cellular localisation with forming or matured MI/MII stage meiotic spindles (Fig. S6). Collectively, these data
380 confirm a novel *Wwc2* role in regulating appropriate chromosome segregation and cell division during mouse oocyte
381 maturation (associated with activation of the key spindle-associated regulatory kinase AURKA); displaying
382 functional conservation with that observed in similarly acentrosomal mitotic cleavage divisions of preimplantation
383 stage embryo blastomeres.
384
385 **siRNA mediated *Wwc2* KD affects blastocyst cell-fate.**
386 Embryo cell number deficits and defective division phenotypes were first evident after global (siRNA) *Wwc2*
387 KD around the 8- to 16-cell stage (Figs. 2 & 3), with clonal *Wwc2* KD (dsRNA) being associated with reduced inner-
388 cell clone numbers (Fig. 1c). Transition from the 8- to 16-cell stage represents the first developmental point embryo
389 blastomeres are overtly distinct in terms of intra-cellular apical-basolateral polarity and relative spatial positioning,
390 with consequences for ultimate blastocyst cell-fate (*i.e.* polarised outer-cells that can give rise to both TE and further
391 inner-cells, plus apolar inner ICM progenitors (Johnson and Ziomek, 1981)).Therefore, we assayed if clonal *Wwc2*
392 KD (siRNA) altered TE versus ICM fate in 32-cell stage equivalent blastocysts, by creating stably marked *Wwc2* KD
393 and control cell clones (expressing recombinant GAP43-GFP as an injection membrane marker; microinjecting one
394 blastomere at the 2-cell stage) and assaying expression of the Hippo-sensitive TE marker CDX2 (Strumpf et al.,
395 2005) (Fig. 6). Control siRNA embryos developed appropriately to form blastocysts containing an average of 59%
396 outer (CDX2 positive) and 41% inner (CDX2 negative) cell populations, with statistically equal contributions from
397 each clone (either control siRNA microinjected or non-microinjected derived). As expected, *Wwc2* siRNA
398 microinjected embryos had significantly fewer cells and the microinjected clone exhibited abnormal nuclear
399 morphologies and a robustly significant impaired ICM contribution; on average 1.6±0.2 cells versus 6.8±0.3 in the
400 non-microinjected clone (or 7.3±0.4 or 7.4±0.3 in the equivalent control siRNA embryo clones, respectively). Clonal
401 TE contribution was also significantly impaired but to a lesser degree (overall TE numbers being compensated by

402 increased non-microinjected clone contribution). Small numbers of outer-cell *Wwc2* KD clones failed to express
403 CDX2 (~20%; not observed in control embryos) with the remainder exhibiting reduced immunoreactivity as
404 compared to the non-microinjected clone (or either clone in control siRNA groups; concurrently IF stained and
405 imaged; Fig. 6b). However, no ectopic inner-cell CDX2 expression within *Wwc2* KD clones was observed and non-
406 microinjected sister clones appropriately expressed CDX2 in outer-cells only. Consequently, in *Wwc2* siRNA
407 microinjected embryos the overall composition of outer versus inner-cells was skewed in favour of outer TE (largely
408 CDX2 positive – 72%) over ICM (exclusively CDX2 negative - 28%). These results suggest that outer-cell Hippo-
409 pathway suppression (specifying TE) and inner-cell activation (preventing TE differentiation and promoting
410 pluripotency) are predominately intact within *Wwc2* KD clones, although outer-cell maintenance of TE
411 differentiation is not optimal. Indeed, a lack of overt outer-cell apical polarity defects (assaying PARD6B) or ectopic
412 nuclear exclusion of YAP (a correlate of activated Hippo-signalling (Nishioka et al., 2009)) within *Wwc2* KD outer
413 blastomeres (Fig. S7) support this conclusion. Although interestingly, YAP nuclear exclusion in inner- *Wwc2* KD
414 cells was consistently less robust than in control siRNA microinjected inner-cells; indicating potential impairment of
415 inner-cell Hippo-signalling activation (Fig. S7 – although note, observed nuclear YAP was far from equivalent to
416 outer residing blastomeres).

417 We extended the IF staining analyses to late blastocysts (E4.5), assaying TE and EPI (CDX2 & NANOG) or
418 PrE and EPI markers (GATA4 & NANOG or GATA4 & SOX2) as pairwise combinations (Figs. 7 & S8). *Wwc2* KD
419 clone specific cell number (plus total blastocyst cell number) deficits, nuclear morphology and cell division
420 phenotypes were again observed. However, in contrast to early blastocysts, the ratio of total outer (TE) to inner (ICM)
421 cells was not significantly different between *Wwc2* and control siRNA microinjection groups (assayed across all
422 lineage combinations; Fig. 7d-f; note, data shown as pie charts to emphasise similar TE:ICM ratios in embryos with
423 significantly different numbers of cells – see Fig. S8 for bar charts of absolute numbers); indicative of regulative
424 development during blastocyst maturation. However, the incidence of fragmented nuclei, consistent with apoptosis,
425 was significantly higher within the *Wwc2* siRNA microinjected clones of the ICM, versus equivalent control siRNA
426 clones (Fig. 7b). Consistently, the overall and significantly reduced contributions of *Wwc2* siRNA clones were more
427 pronounced for ICM versus outer-cell populations (Fig. S8). Focussing, on CDX2 and NANOG stained groups, a
428 population of CDX2 negative outer-cells and generally reduced CDX2 expression within the *Wwc2* KD outer-
429 residing clone was again observed (Fig. 7c). Interestingly, the significantly reduced *Wwc2* KD clone derived ICM
430 cell numbers did not segregate, as per marked control siRNA clones, between NANOG positive (indicative of EPI)
431 and NANOG negative (potentially PrE) populations. Rather, they were biased towards NANOG negative cells,
432 representative of potential PrE (Fig. 7d; again note data represented as pie charts to emphasise differences in the
433 clonal contribution to EPI and PrE ICM lineages in embryos with significantly different numbers of cells – see Fig.
434 S8 for bar charts of absolute numbers in each assayed ICM lineage). Considering all assayed embryos together, the
435 overall reductions in potential PrE (NANOG negative) population size (associated with clonal *Wwc2* KD), were
436 substantially smaller than that observed for the EPI (Fig. S8); further suggesting inner *Wwc2* KD clones are impaired
437 in their sustained contribution to the EPI but are more able to differentiate into PrE. Data from directly assaying the
438 two ICM lineages together (GATA4 & NANOG or SOX2; Figs. 7e & f, plus Fig. S8) also demonstrated
439 characteristically low numbers of inner *Wwc2* KD clones, similarly segregated in favour of the PrE over EPI
440 (although compensatory increases in EPI contribution from non-microinjected clones were noted - Fig. S8).

441 Numerous examples of SOX2 positive fragmented inner-cell nuclei within the *Wwc2* KD clone were also noted
442 (Fig.7c); indicating the observed increased incidence of apoptosis (Fig. 7b) was centred on specified EPI that was
443 unable to be maintained (note, reliable quantification of SOX2 positive apoptotic nuclei was not possible).
444 Interestingly, we noted a small population of marked ICM *Wwc2* KD clones expressing neither PrE or EPI markers
445 (4.6% of all ICM cells and 18.7% of the clone - not present in controls), potentially indicative of further ICM cell-
446 fate defects.
447 In summary, these data confirm *Wwc2* KD clone specific and autonomous reductions in overall embryo cell
448 number that more robustly affect formation of ICM versus TE (compensated by regulation within the non-injected
449 clone to preserve the overall TE:ICM ratio at the late blastocyst stage; albeit with fewer overall cells). Moreover,
450 ICM lineage contribution of *Wwc2* KD clones is also biased against the pluripotent EPI and favours PrE
451 differentiation, potentially via a mechanism involving selective apoptosis of specified EPI. Thus, uncovering a
452 blastocyst cell-fate role of *Wwc2* that is additional to that related to cell division.
453
454 **Embryo *Wwc2* siRNA KD phenotypes are reversible by recombinant HA-WWC2 protein expression.**
455 To confirm the uncovered embryo related roles of *Wwc2*, we attempted phenotypic rescue experiments using
456 the same recombinant siRNA-resistant *HA-Wwc2* mRNA construct described above (oocyte IVM – Fig. 5). We
457 therefore repeated the marked clonal microinjection experiments but included a third condition in which *Wwc2*
458 siRNA was co-microinjected with *HA-Wwc2* mRNA. Total and clonal cell contributions to inner and outer-cell
459 populations, plus the incidence of abnormal nuclear morphology, were calculated in early and late blastocysts (Fig.
460 8). Embryos microinjected with *Wwc2* siRNA alone exhibited the typical clone autonomous phenotypes. However,
461 under *Wwc2* siRNA conditions supplemented with co-microinjected *HA-Wwc2* mRNA (expression of which was
462 confirmed, see below and Fig. 8d) the average cell number, clonal and spatial composition of constituent early and
463 late blastocysts was statistically indistinguishable from control siRNA microinjection groups (except for a small
464 reduction in ICM contribution of the non-microinjected clone at the late blastocyst stage - from 9.5±0.4 to 8.2±0.3).
465 Additionally, a near complete rescue of abnormal morphologies was observed (only one exception across all
466 blastomeres assayed – shown in Fig. 8c & d). These data demonstrate the specificity of the employed siRNA and
467 confirm *Wwc2* as a novel regulatory gene of embryo cell division and subsequent cell-fate.
468 Incorporation of a HA-epitope tag within the confirmed *HA-Wwc2* phenotypic rescue mRNA enabled IF
469 mediated verification of its translation and provided information on protein sub-cellular localisation within the
470 microinjected clone. We consistently detected specific anti-HA immuno-reactivity (not observed either control or
471 *Wwc2* siRNA microinjected embryos) at structures resembling mitotic spindle mid-bodies, particularly evident within
472 microinjected clones at the 32-cell stage (Fig. 8d & Fig. S9a). A recent study identified a critical role for
473 uncharacteristically persistent interphase mid-bodies (referred to as 'interphase microtubule bridges') as important
474 MTOCs within cleavage stage blastomeres (Zenker et al., 2017). Therefore, we assayed their number, IF-staining for
475 α-Tubulin and activated phospho-Aurora-B (pAURKB) as recognised midbody markers (Terada et al., 1998), in
476 control and *Wwc2* KD embryos at the same 32-cell stage, but could not detect any statistically significant variation
477 in their incidence (when corrected for reduced cell number caused by *Wwc2* KD - Fig. S9c-e). Hence, whilst *HA-*
478 *Wwc2* derived recombinant protein associates with cell division mid-bodies, the removal of endogenous *Wwc2*
479 mRNA does not appear to impair mid-body formation or persistence following compromised cell divisions.

480

481 **DISCUSSION**

482

483 We have identified *Wwc2*, the sole murine WWC-domain containing paralog of the recognised Hippo-
484 pathway activator *Kibra* (Baumgartner et al., 2010;Genevet et al., 2010;Yu et al., 2010;Xiao et al., 2011a;Wennmann
485 et al., 2014), as a novel regulator of preimplantation mouse embryo mitotic cell cleavages (Figs. 1-3) and oocyte
486 meiotic maturation (Fig. 4); the latter predicated on appropriate activation of AURKA (Figs. 5 and S6). Additionally,
487 in the embryo we show *Wwc2* KD cell clones are compromised in EPI lineage contribution and are prone to apoptosis
488 or disproportionate PrE contribution (Figs. 6 & 7 and S8). These data implicate at least two functional roles for *Wwc2*
489 during early mouse development/reproduction; i) spatial and temporal regulation of germane meiotic and mitotic cell
490 divisions (paradigms of typical and atypical acentrosomal cell division, relative to other mammalian species,
491 respectively (Courtois et al., 2012;Bennabi et al., 2016;Severson et al., 2016;Gruss, 2018;Mogessie et al.,
492 2018;Namgoong and Kim, 2018)), and ii) influencing blastomere pluripotency and differentiation, particularly
493 relating to EPI and PrE formation (Figs. 6 & 7 and S8). However, the full extent of the cell-fate related role is difficult
494 to experimentally dissect, given the described cell division defects, evident as early as the 8-cell stage.
495 Regarding cell-fate regulation, active Hippo-signalling is known to support initial pluripotency and resist TE
496 differentiation in ICM founders, by blocking YAP nuclear localisation (Sasaki, 2017). However, recently it has been
497 shown nuclear that YAP translocation is later required for blastocyst EPI progenitors to compete with each other to
498 achieve optimal naïve pluripotency (Hashimoto and Sasaki, 2019). Hence, depending on developmental context,
499 active Hippo-signalling appears to both initially promote and latterly suppress relative pluripotency status. Our data,
500 although compounded by the additional cell division phenotypes, suggests *Wwc2* (as a paralog of the known Hippo-
501 activator *Kibra* (Baumgartner et al., 2010;Genevet et al., 2010;Yu et al., 2010;Xiao et al., 2011a)) may contribute to
502 germane Hippo-signalling mediated regulation of pluripotency. For example, we find ICM-residing late blastocyst
503 *Wwc2* KD clones, although fewer than their non-microinjected clone counterparts, statistically favour contribution
504 to PrE over EPI (unlike in control groups); indicative of impaired pluripotent potential (Figs. 6 & 7 and S8). Whether
505 this is caused by compromised Hippo-signalling activation directly after initial ICM founder internalisation or is
506 related to an inability to successfully compete for naïve pluripotency in the EPI, is not clear. However, increased
507 apoptosis within ICM residing *Wwc2* KD clones, often marked by detectable SOX2 protein expression (but never
508 GATA4 - Fig. 7b & c) is consistent with the competitive elimination of initially pluripotent EPI progenitors unable
509 to achieve/compete for, naïve pluripotency. Indeed, analysis of early blastocyst stage *Wwc2* KD embryos/clones,
510 suggests the establishment of required differential Hippo-signalling between TE (*i.e.* suppression) and ICM (*i.e.*
511 activation) was largely intact (Figs. 6 and S7; see CDX2, PARD6B, CDH1 and YAP IF staining). Although,
512 comparatively reduced (or sometimes absent) outer-cell CDX2 expression, plus less efficient inner-cell YAP protein
513 nuclear exclusion, in *Wwc2* KD clones (Figs. 6 & 7 and S7) implies a degree of early onset mild Hippo-signalling
514 dysregulation; potentially becoming more manifest during blastocyst maturation. EPI specific exclusion of *Wwc2*
515 KD clones may also be related to increased aneuploidy caused by defective cell divisions, as derived experimental
516 clonal aneuploidy in mouse chimeras is known to be selectively eliminated from the EPI by apoptosis but tolerated
517 within extra-embryonic blastocyst tissues (Bolton et al., 2016). The mild early cell-fate effects may also reflect
518 functional redundancy between WWC2 and KIBRA; indeed, robust *Wwc2* KD does not affect *Kibra* mRNA levels

519 (Fig. 1 and S1). Functional redundancy between WWC-domain proteins paralogs has been demonstrated in human
520 cells (relating to KIBRA, WWC2 and WWC3 (Wennmann et al., 2014)) and genetic ablation of the mouse *Kibra*
521 gene is developmentally viable (adult mice only exhibit minor learning and memory defects (Makuch et al., 2011)).
522 However, if KIBRA and WWC2 proteins share functional redundancy during mouse preimplantation development,
523 it is probably only in relation to potential Hippo-signalling regulation and not applicable to the described cell division
524 functions of *Wwc2* (as sole *Kibra* KD did not affect cell number – Fig. 1).
525 Given *Wwc2* specific siRNA embryo microinjections were performed at the 2-cell stage it is unclear why
526 cell autonomous division phenotypes (particularly affecting inner-cell populations) are only manifest by the 16-cell
527 stage (Figs. 1 - 3 and S2). One possibility is that all post-microinjection cell-cycles are elongated in a manner only
528 revealed at the whole embryo level by the 16-cell stage, implicating *Wwc2* as a regulator of the atypically long cell-
529 cycles of preimplantation mammalian embryo blastomeres (reviewed (O'Farrell et al., 2004)). Alternatively, it may
530 reflect functional exhaustion of maternally provided WWC2 protein, unaffected by siRNA (although, it was
531 impossible to directly assay WWC2 protein expression, due to unavailability of antibodies). The emergence of
532 phenotypes at the 16-cell stage also coincides with the first spatial segregation of blastomeres (outer- and inner-
533 positions), polarity/position dependant differential Hippo-signalling establishment and TE versus ICM cell-fate
534 formation (Sasaki, 2017). It is tempting to speculate such developmental timing is particularly relevant in this context.
535 However, the onset of individual nuclear morphological phenotypes, indicative of defective cell division/cytokinesis
536 (mid-body association, bi-/multi-/micro-nucleation - Fig. 3), were already evident by the 8-cell stage. Additionally,
537 although weak, outer-cell restricted CDX2 protein expression confirmed intact differential Hippo-signalling (Fig. 6
538 & 7). Interestingly, whilst average cell number was impaired by *Wwc2* KD after the 8-cell stage, we noted it did not
539 significantly increase again until the mid-blastocyst stage (remaining around 8-10 cells - Fig. 2). Significantly, the
540 mid-blastocyst stage marks the developmental point that atypical (compared to most other mammalian species)
541 mouse embryo acentrosomal cell divisions revert back to centrosomal control, after *de novo* centrosome synthesis
542 (Courtois et al., 2012). We propose our data invoke a role for WWC2 in regulating mouse preimplantation stage
543 acentrosomal blastomere cleavage, supported by the uncovered nuclear morphology phenotypes associated with
544 *Wwc2* KD (Fig. 3) and readily detectable recombinant HA-WWC2 protein in mitotic mid-bodies up until the early
545 blastocyst stage (not easily detectable in late blastocysts - Figs. 8 and S9). We suspect HA-WWC2 association with
546 mid-bodies reflects a role for WWC2 during preceeding cell divisions and that the localisation represents a remant
547 of this role rather than affecting the previously described MTOC function of such atypically persistent mouse
548 cleavage blastomere mid-bodies (Zenker et al., 2017); indeed, when corrected for lower overall cell numbers, the
549 total number of detectable mid-bodies is not significantly different in *Wwc2* KD embryos from controls (Fig. S9).
550 Moreover, the impaired oocyte maturation data, by which GV oocytes (again in the absence of centrosomes (Bennabi
551 et al., 2016;Severson et al., 2016;Gruss, 2018;Mogessie et al., 2018;Namgoong and Kim, 2018)) depleted of *Wwc2*
552 transcripts present with multiple spindle defects associated with failed AURKA activation (Figs. 4 & 5 and S3 &
553 S6), further substantiates this hypothesis. Interestingly, clonal *Aurkb* and *Aurkc* downregulation in preimplantation
554 mouse embryos, respectively increases or decreases the rate of mitotic cell division (over-expression exhibiting the
555 opposing effects). Indeed, the reported cell number deficits associated with *Aurkc* downregulation, strongly resemble
556 those associated with *Wwc2* KD (Li et al., 2017), suggesting a potential link between WWC2 and AURKB/AURKC
557 function in the early embryo.

558 Regulation of mammalian Hippo-signalling by WWC-domain proteins was first demonstrated in human
559 HEK293T cells, whereby direct binding of KIBRA was shown to activate LATS1/2, causing YAP phosphorylation
560 (Xiao et al., 2011a). A subsequent report detailed AURKA/B directed and mitosis specific KIBRA phosphorylation,
561 centred on a conserved Ser539 residue, and showed the KIBRA mutant (S539A) promotes precocious M-phase exit
562 in models of spindle assembly check-point (SAC) mediated arrest (Xiao et al., 2011b). The same group later
563 demonstrated full activation/phosphorylation of AURKA (hence, LATS2 activation and appropriate centrosomal
564 localisation) requires KIBRA and that *KIBRA* KD causes spindle defects, lagging chromosomes and micronuclei
565 formation (reminiscent of our uncovered *Wwc2* KD phenotypes), plus centrosomal fragmentation in human cell line
566 models (Zhang et al., 2012). Interestingly, we have identified conserved AURK consensus motifs in both murine
567 KIBRA and WWC2 proteins; including those paralogous to Ser539 (Fig. S10). We therefore hypothesise the *Wwc2*
568 KD phenotypes we observe here are mechanistically related to those described for human KIBRA, with the caveat
569 they function on the level of MTOC regulation due to the absence of centrosomes (Courtois et al., 2012). For example,
570 genetic ablations of either murine *Lats1* and *Lats2*, do not cause embryo cell number deficits typical of *Wwc2* KD,
571 nor those centrosome directed mitotic phenotypes described above, rather presenting in early blastocysts as ectopic
572 ICM cell nuclear YAP localisations (Nishioka et al., 2009). Therefore, not all insights will be directly transferable.
573 Notwithstanding and despite the lack of early mouse embryo centrosomes, key centrosome regulators are expressed
574 and reported to regulate embryo cleavage divisions. For example, genetic knockout of Polo-like kinase 1 (*Plk1*),
575 known to cooperate with AURKA within centrosomes to mediated bi-polar spindle formation (Asteriti et al., 2015),
576 causes arrest at the same 8-cell stage at which global *Wwc2* KD embryos first exhibit cell division defects (Figs. 2
577 and 3) (Lu et al., 2008). Moreover, an important role in blastomere division for the related *Plk4* gene, itself recognised
578 as a key regulator of centriole formation/duplication (Bettencourt-Dias et al., 2005;Habedanck et al., 2005), has been
579 demonstrated. Accordingly, active PLK4 protein localises to chromatin proximal and coalescing MTOCs to promote
580 microtubule nucleation and bi-polar spindle formation (Coelho et al., 2013). It will be interesting to investigate the
581 identified *Wwc2* KD phenotypes in the context of such pre-existing and characterised MTOC-related factors and to
582 test their applicability within the conceptually similar paradigm of acentrosomal meiotic oocyte maturation. Indeed,
583 upon resumption of meiosis, PLK4 was recently described to cooperate with AURKA (within MTOCs) to initiate
584 microtubule nucleation around condensing chromosomes. Functional inhibition of PLK4 did not however block
585 spindle assembly but increased assembly time and the individual MTOC regulatory roles of PLK4 and AURKA were
586 shown to be only partially overlapping (Bury et al., 2017) and distinct from the co-existing chromosome derived
587 RAN-GTP gradient driven mechanisms (as reviewed (Bennabi et al., 2016;Severson et al., 2016;Gruss,
588 2018;Mogessie et al., 2018;Namgoong and Kim, 2018)). Importantly, the described functional inhibition of PLK4
589 was associated with eventual polar body formation (Bury et al., 2017), unlike after *Wwc2* KD (even after an extended
590 IVM incubation time – Fig. S3). This indicates that whilst meiotic spindle assembly is impaired to varying degrees
591 by *Wwc2* KD (Fig. 4d & d'), other impediments to successful meiotic maturation must exist (potentially relating,
592 although not necessarily limited, to spindle migration, SAC, cytokinesis *etc.*). The comparative distribution of
593 observed meiotic maturation phenotypes caused by *Wwc2* KD (*i.e.* failed spindle formation, defective spindles or
594 persistent/ non-dividing MI spindles – Fig. 4d & d') suggests some functional redundancy in response to loss of
595 WWC2. This may be potentially related to the compensatory abilities of the three expressed AURK paralogs (*Aurka*,
596 *Aurkb* and *Aurkc*), as demonstrated in combinatorial genetic ablations in mouse oocytes (Nguyen et al., 2018).

In summary, we have identified the ill-characterised WWC-domain containing gene *Wwc2,* as an important regulator of cell division in both preimplantation mouse embryo blastomeres and oocytes; both paradigms of acentrosomal cell division. We have also uncovered evidence for *Wwc2,* as a paralog of the described Hippo-signalling activator *Kibra*, in participating in blastocyst cell-fate regulation and pluripotency. Despite the compounding nature of the two identified *Wwc2* KD phenotypes, it will be of great future interest to further our molecular understanding of these newly identified roles of the *Wwc2* gene during early mouse development.

ACKNOWLEDGEMENTS

Authors acknowledge Marta Gajewska (Institute of Oncology, Warsaw, Poland) and Anna Piliszek (Institute of Genetics & Animal Breeding, Polish Academy of Sciences, Jastrzębiec, Poland) for providing founder CBA/W mice used in this study, Martin Anger (Central European Institute of Technology (CEITEC)/ Veterinary Research Institute, Brno, Czech Republic) for valuable technical advice and discussions and Alena Krejčí (Faculty of Science, University of South Bohemia, České Budějovice, Czech Republic) for advice and pooling resources. The Animal Facility (Institute of Parasitology, Biology Centre of the Czech Academy of Sciences, České Budějovice, Czech Republic) is acknowledged for housing experimental mice. The research was supported by a Czech Science Foundation/ GA ČR grant (18-02891S) awarded to A.W.B. and a Grant Agency of the University of South Bohemia Ph.D. student award to G.V (GA JU: 015/2017/P).

CONFLICT OF INTEREST

The authors declare that they have no conflict of interests.

REFERENCES

Asteriti, I.A., De Mattia, F., and Guarguaglini, G. (2015). Cross-Talk between AURKA and Plk1 in Mitotic Entry and Spindle Assembly. *Front Oncol* 5**,** 283.

Baumgartner, R., Poernbacher, I., Buser, N., Hafen, E., and Stocker, H. (2010). The WW domain protein Kibra acts upstream of Hippo in Drosophila. *Dev Cell* 18**,** 309-316.

Bennabi, I., Terret, M.E., and Verlhac, M.H. (2016). Meiotic spindle assembly and chromosome segregation in oocytes. *J Cell Biol* 215**,** 611-619.

Bettencourt-Dias, M., Rodrigues-Martins, A., Carpenter, L., Riparbelli, M., Lehmann, L., Gatt, M.K., Carmo, N., Balloux, F., Callaini, G., and Glover, D.M. (2005). SAK/PLK4 is required for centriole duplication and flagella development. *Curr Biol* 15**,** 2199-2207.

Bolton, H., Graham, S.J.L., Van Der Aa, N., Kumar, P., Theunis, K., Fernandez Gallardo, E., Voet, T., and Zernicka-Goetz, M. (2016). Mouse model of chromosome mosaicism reveals lineage-specific depletion of aneuploid cells and normal developmental potential. *Nat Commun* 7**,** 11165.

Bury, L., Coelho, P.A., Simeone, A., Ferries, S., Eyers, C.E., Eyers, P.A., Zernicka-Goetz, M., and Glover, D.M. (2017). Plk4 and Aurora A cooperate in the initiation of acentriolar spindle assembly in mammalian oocytes. *J Cell Biol* 216**,** 3571-3590.

Chazaud, C., and Yamanaka, Y. (2016). Lineage specification in the mouse preimplantation embryo. *Development* 143**,** 1063-1074.

Coelho, P.A., Bury, L., Sharif, B., Riparbelli, M.G., Fu, J., Callaini, G., Glover, D.M., and Zernicka-Goetz, M. (2013). Spindle formation in the mouse embryo requires Plk4 in the absence of centrioles. *Dev Cell* 27**,** 586-597.

Courtois, A., Schuh, M., Ellenberg, J., and Hiiragi, T. (2012). The transition from meiotic to mitotic spindle assembly is gradual during early mammalian development. *J Cell Biol* 198**,** 357-370.

Davis, J.R., and Tapon, N. (2019). Hippo signalling during development. *Development* 146.

Frum, T., Murphy, T.M., and Ralston, A. (2018). HIPPO signaling resolves embryonic cell fate conflicts during establishment of pluripotency in vivo. *Elife* 7.

Frum, T., and Ralston, A. (2015). Cell signaling and transcription factors regulating cell fate during formation of the mouse blastocyst. *Trends Genet* 31**,** 402-410.

Frum, T., Watts, J.L., and Ralston, A. (2019). TEAD4, YAP1 and WWTR1 prevent the premature onset of pluripotency prior to the 16-cell stage. *Development* 146.

Genevet, A., Wehr, M.C., Brain, R., Thompson, B.J., and Tapon, N. (2010). Kibra is a regulator of the Salvador/Warts/Hippo signaling network. *Dev Cell* 18**,** 300-308.

Gruss, O.J. (2018). Animal Female Meiosis: The Challenges of Eliminating Centrosomes. *Cells* 7.

Habedanck, R., Stierhof, Y.D., Wilkinson, C.J., and Nigg, E.A. (2005). The Polo kinase Plk4 functions in centriole duplication. *Nat Cell Biol* 7**,** 1140-1146.

Han, Q., Kremerskothen, J., Lin, X., Zhang, X., Rong, X., Zhang, D., and Wang, E. (2018). WWC3 inhibits epithelial-mesenchymal transition of lung cancer by activating Hippo-YAP signaling. *Onco Targets Ther* 11**,** 2581-2591.

Hashimoto, M., and Sasaki, H. (2019). Epiblast Formation by TEAD-YAP-Dependent Expression of Pluripotency Factors and Competitive Elimination of Unspecified Cells. *Dev Cell* 50**,** 139-154 e135.

Hassold, T., and Hunt, P. (2001). To err (meiotically) is human: the genesis of human aneuploidy. *Nat Rev Genet* 2**,** 280-291.

Hirate, Y., Hirahara, S., Inoue, K., Kiyonari, H., Niwa, H., and Sasaki, H. (2015). Par-aPKC-dependent and -independent mechanisms cooperatively control cell polarity, Hippo signaling, and cell positioning in 16-cell stage mouse embryos. *Dev Growth Differ* 57**,** 544-556.

Horn, T., and Boutros, M. (2010). E-RNAi: a web application for the multi-species design of RNAi reagents--2010 update. *Nucleic Acids Res* 38**,** W332-339.

Johnson, M.H., and Ziomek, C.A. (1981). The foundation of two distinct cell lineages within the mouse morula. *Cell* 24**,** 71-80.

Koncicka, M., Tetkova, A., Jansova, D., Del Llano, E., Gahurova, L., Kracmarova, J., Prokesova, S., Masek, T., Pospisek, M., Bruce, A.W., Kubelka, M., and Susor, A. (2018). Increased Expression of Maturation Promoting Factor Components Speeds Up Meiosis in Oocytes from Aged Females. *Int J Mol Sci* 19.

674 Kovarikova, V., Burkus, J., Rehak, P., Brzakova, A., Solc, P., and Baran, V. (2016). Aurora kinase A is
675 essential for correct chromosome segregation in mouse zygote. *Zygote* 24**,** 326-337.
676 Lemaire, P., Garrett, N., and Gurdon, J.B. (1995). Expression cloning of Siamois, a Xenopus homeobox
677 gene expressed in dorsal-vegetal cells of blastulae and able to induce a complete secondary
678 axis. *Cell* 81**,** 85-94.
679 Li, W., Wang, P., Zhang, B., Zhang, J., Ming, J., Xie, W., and Na, J. (2017). Differential regulation of
680 H3S10 phosphorylation, mitosis progression and cell fate by Aurora Kinase B and C in mouse
681 preimplantation embryos. *Protein Cell* 8**,** 662-674.
682 Livak, K.J., and Schmittgen, T.D. (2001). Analysis of relative gene expression data using real-time
683 quantitative PCR and the 2(-Delta Delta C(T)) Method. *Methods* 25**,** 402-408.
684 Lu, L.Y., Wood, J.L., Minter-Dykhouse, K., Ye, L., Saunders, T.L., Yu, X., and Chen, J. (2008). Polo-like
685 kinase 1 is essential for early embryonic development and tumor suppression. *Mol Cell Biol* 28**,**
686 6870-6876.
687 Makuch, L., Volk, L., Anggono, V., Johnson, R.C., Yu, Y., Duning, K., Kremerskothen, J., Xia, J.,
688 Takamiya, K., and Huganir, R.L. (2011). Regulation of AMPA receptor function by the human
689 memory-associated gene KIBRA. *Neuron* 71**,** 1022-1029.
690 Mihajlovic, A.I., and Bruce, A.W. (2016). Rho-associated protein kinase regulates subcellular localisation
691 of Angiomotin and Hippo-signalling during preimplantation mouse embryo development. *Reprod*
692 *Biomed Online* 33**,** 381-390.
693 Mihajlovic, A.I., and Bruce, A.W. (2017). The first cell-fate decision of mouse preimplantation embryo
694 development: integrating cell position and polarity. *Open Biol* 7.
695 Mihajlovic, A.I., and Fitzharris, G. (2018). Segregating Chromosomes in the Mammalian Oocyte. *Curr*
696 *Biol* 28**,** R895-R907.
697 Mihajlovic, A.I., Thamodaran, V., and Bruce, A.W. (2015). The first two cell-fate decisions of
698 preimplantation mouse embryo development are not functionally independent. *Sci Rep* 5**,** 15034.
699 Mogessie, B., Scheffler, K., and Schuh, M. (2018). Assembly and Positioning of the Oocyte Meiotic
700 Spindle. *Annu Rev Cell Dev Biol* 34**,** 381-403.
701 Morris, S.A., Teo, R.T., Li, H., Robson, P., Glover, D.M., and Zernicka-Goetz, M. (2010). Origin and
702 formation of the first two distinct cell types of the inner cell mass in the mouse embryo. *Proc Natl*
703 *Acad Sci U S A* 107**,** 6364-6369.
704 Nagaoka, S.I., Hassold, T.J., and Hunt, P.A. (2012). Human aneuploidy: mechanisms and new insights
705 into an age-old problem. *Nat Rev Genet* 13**,** 493-504.
706 Namgoong, S., and Kim, N.H. (2018). Meiotic spindle formation in mammalian oocytes: implications for
707 human infertility. *Biol Reprod* 98**,** 153-161.
708 Nguyen, A.L., Drutovic, D., Vazquez, B.N., El Yakoubi, W., Gentilello, A.S., Malumbres, M., Solc, P., and
709 Schindler, K. (2018). Genetic Interactions between the Aurora Kinases Reveal New
710 Requirements for AURKB and AURKC during Oocyte Meiosis. *Curr Biol* 28**,** 3458-3468 e3455.
711 Nguyen, A.L., and Schindler, K. (2017). Specialize and Divide (Twice): Functions of Three Aurora Kinase
712 Homologs in Mammalian Oocyte Meiotic Maturation. *Trends Genet* 33**,** 349-363.
713 Nishioka, N., Inoue, K., Adachi, K., Kiyonari, H., Ota, M., Ralston, A., Yabuta, N., Hirahara, S.,
714 Stephenson, R.O., Ogonuki, N., Makita, R., Kurihara, H., Morin-Kensicki, E.M., Nojima, H.,
715 Rossant, J., Nakao, K., Niwa, H., and Sasaki, H. (2009). The Hippo signaling pathway
716 components Lats and Yap pattern Tead4 activity to distinguish mouse trophectoderm from inner
717 cell mass. *Dev Cell* 16**,** 398-410.
718 O'farrell, P.H., Stumpff, J., and Su, T.T. (2004). Embryonic cleavage cycles: how is a mouse like a fly?
719 *Curr Biol* 14**,** R35-45.
720 Rossant, J. (2016). Making the Mouse Blastocyst: Past, Present, and Future. *Curr Top Dev Biol* 117**,**
721 275-288.
722 Rossant, J. (2018). Genetic Control of Early Cell Lineages in the Mammalian Embryo. *Annu Rev Genet*
723 52**,** 185-201.
724 Salles, F.J., Darrow, A.L., O'connell, M.L., and Strickland, S. (1992). Isolation of novel murine maternal
725 mRNAs regulated by cytoplasmic polyadenylation. *Genes Dev* 6**,** 1202-1212.
726 Sanders, J.R., and Jones, K.T. (2018). Regulation of the meiotic divisions of mammalian oocytes and
727 eggs. *Biochem Soc Trans* 46**,** 797-806.
728 Sasaki, H. (2017). Roles and regulations of Hippo signaling during preimplantation mouse development.
729 *Dev Growth Differ* 59**,** 12-20.

730 Saskova, A., Solc, P., Baran, V., Kubelka, M., Schultz, R.M., and Motlik, J. (2008). Aurora kinase A
731 controls meiosis I progression in mouse oocytes. *Cell Cycle* 7**,** 2368-2376.
732 Sathananthan, A.H., Kola, I., Osborne, J., Trounson, A., Ng, S.C., Bongso, A., and Ratnam, S.S. (1991).
733 Centrioles in the beginning of human development. *Proc Natl Acad Sci U S A* 88**,** 4806-4810.
734 Schatten, H., and Sun, Q.Y. (2009). The role of centrosomes in mammalian fertilization and its
735 significance for ICSI. *Mol Hum Reprod* 15**,** 531-538.
736 Severson, A.F., Von Dassow, G., and Bowerman, B. (2016). Oocyte Meiotic Spindle Assembly and
737 Function. *Curr Top Dev Biol* 116**,** 65-98.
738 Solc, P., Baran, V., Mayer, A., Bohmova, T., Panenkova-Havlova, G., Saskova, A., Schultz, R.M., and
739 Motlik, J. (2012). Aurora kinase A drives MTOC biogenesis but does not trigger resumption of
740 meiosis in mouse oocytes matured in vivo. *Biol Reprod* 87**,** 85.
741 Strumpf, D., Mao, C.A., Yamanaka, Y., Ralston, A., Chawengsaksophak, K., Beck, F., and Rossant, J.
742 (2005). Cdx2 is required for correct cell fate specification and differentiation of trophectoderm in
743 the mouse blastocyst. *Development* 132**,** 2093-2102.
744 Swain, J.E., Ding, J., Wu, J., and Smith, G.D. (2008). Regulation of spindle and chromatin dynamics
745 during early and late stages of oocyte maturation by aurora kinases. *Mol Hum Reprod* 14**,** 291-
746 299.
747 Terada, Y., Tatsuka, M., Suzuki, F., Yasuda, Y., Fujita, S., and Otsu, M. (1998). AIM-1: a mammalian
748 midbody-associated protein required for cytokinesis. *EMBO J* 17**,** 667-676.
749 Wang, Q.T., Piotrowska, K., Ciemerych, M.A., Milenkovic, L., Scott, M.P. Davis, R.W., and Zernicka-
750 Goetz, M. (2004). A genome-wide study of gene activity reveals developmental signaling
751 pathways in the preimplantation mouse embryo. *Dev Cell* 6, 133-144.
752 Wennmann, D.O., Schmitz, J., Wehr, M.C., Krahn, M.P., Koschmal, N., Gromnitza, S., Schulze, U.,
753 Weide, T., Chekuri, A., Skryabin, B.V., Gerke, V., Pavenstadt, H., Duning, K., and
754 Kremerskothen, J. (2014). Evolutionary and molecular facts link the WWC protein family to Hippo
755 signaling. *Mol Biol Evol* 31**,** 1710-1723.
756 White, M.D., Zenker, J., Bissiere, S., and Plachta, N. (2018). Instructions for Assembling the Early
757 Mammalian Embryo. *Dev Cell* 45**,** 667-679.
758 Wicklow, E., Blij, S., Frum, T., Hirate, Y., Lang, R.A., Sasaki, H., and Ralston, A. (2014). HIPPO pathway
759 members restrict SOX2 to the inner cell mass where it promotes ICM fates in the mouse
760 blastocyst. *PLoS Genet* 10**,** e1004618.
761 Xiao, L., Chen, Y., Ji, M., and Dong, J. (2011a). KIBRA regulates Hippo signaling activity via interactions
762 with large tumor suppressor kinases. *J Biol Chem* 286**,** 7788-7796.
763 Xiao, L., Chen, Y., Ji, M., Volle, D.J., Lewis, R.E., Tsai, M.Y., and Dong, J. (2011b). KIBRA protein
764 phosphorylation is regulated by mitotic kinase aurora and protein phosphatase 1. *J Biol Chem*
765 286**,** 36304-36315.
766 Yu, J., Zheng, Y., Dong, J., Klusza, S., Deng, W.M., and Pan, D. (2010). Kibra functions as a tumor
767 suppressor protein that regulates Hippo signaling in conjunction with Merlin and Expanded. *Dev*
768 *Cell* 18**,** 288-299.
769 Zenker, J., White, M.D., Templin, R.M., Parton, R.G., Thorn-Seshold, O., Bissiere, S., and Plachta, N.
770 (2017). A microtubule-organizing center directing intracellular transport in the early mouse
771 embryo. *Science* 357**,** 925-928.
772 Zernicka-Goetz, M., Pines, J., Ryan, K., Siemering, K.R., Haseloff, J., Evans, M.J., and Gurdon, J.B.
773 (1996). An indelible lineage marker for Xenopus using a mutated green fluorescent protein.
774 *Development* 122**,** 3719-3724.
775 Zhang, L., Iyer, J., Chowdhury, A., Ji, M., Xiao, L., Yang, S., Chen, Y., Tsai, M.Y., and Dong, J. (2012).
776 KIBRA regulates aurora kinase activity and is required for precise chromosome alignment during
777 mitosis. *J Biol Chem* 287**,** 34069-34077.
778 Zhang, Y., Yan, S., Chen, J., Gan, C., Chen, D., Li, Y., Wen, J., Kremerskothen, J., Chen, S., Zhang, J.,
779 and Cao, Y. (2017). WWC2 is an independent prognostic factor and prevents invasion via Hippo
780 signalling in hepatocellular carcinoma. *J Cell Mol Med* 21**,** 3718-3729.

781 **FIGURE LEGENDS**

782

783 **Figure 1: dsRNA mediated WWC-domain containing gene (*Kibra* & *Wwc2*) KD in preimplantation mouse**
784 **embryos is associated (*Wwc2*) reduced cell number. a)** Experimental schema of *Kibra* and *Wwc2* specific dsRNA
785 (plus *EGFP n*egative control) microinjection mediated global embryo KD, followed by culture to either 8-cell or 32-
786 cell stages and Q-RT-PCR analysis (upper). Normalised expression of either *Kibra* or *Wwc2* derived mRNAs after
787 stated dsRNA microinjection, at stated developmental stages (lower; error bars represent s.e.m., n=3 and ** denotes
788 p<0.005 in 2-tailed student t-test, n.s. denotes lack of significance). **b)** Experimental schema describing clonal *Kibra*,
789 *Wwc2* or *Kibra+Wwc2* KD (microinjection of one cell at the 2-cell stage) and total fixed embryo cell number assay
790 at the late blastocyst (>64-cell) stage (upper). Average total cell number per embryo in each stated dsRNA
791 microinjection group (lower chart). **c)** Experimental strategy to KD *Wwc2* expression (as in b) in marked clones,
792 (*Wwc2* dsRNA and rhodamine conjugated dextran microbeads/RDBs co-microinjection) and assay clonal
793 contribution at the 16-cell stage (upper). Average total cell number per clone (Inj. vs. Non) in *Wwc2* or control dsRNA
794 microinjection groups, as determined by relative position of individual cells within the embryo (encapsulated inside
795 or with a cell contactless domain on outside; lower chart). In panels b) & c) chart error bars represent s.e.m. with
796 indicated 'n' numbers. Highlighted statistically significant differences (2-tailed students t-test) between experimental
797 microinjection groups (asterisks), or clones (Inj. vs. Non) within a group (double crosses), with statistical confidence
798 intervals of p<0.05 and p<0.005, denoted by one or two significance markers, respectively; in panel b) a lack of
799 significant difference between compared groups is marked 'n.s.'. Supplementary tables ST1 and ST2 summarise
800 statistical analysis and individual embryo data.

801

802 **Figure 2: siRNA mediated global *Wwc2* KD causes persistent preimplantation stage cell number deficits from**
803 **the 8-cell stage. a)** Experimental design; non-specific control or *Wwc2*-specific siRNA co-microinjected with RDBs,
804 into both blastomeres at the 2-cell stage, and cultured, fixed and subject to total cell assay count (including DAPI and
805 phalloidin staining) at indicated developmental stages. A separate group of microinjected embryos were subject to
806 normalised *Wwc2*-specific Q-RTPCR to assay KD efficiency at the 32-cell stage. **b)** Q-RTPCR data of siRNA
807 mediated endogenous *Wwc2* expression KD at the 32-cellstage (error bars denote s.e.m. of triplicate measurements,
808 n=3). **c)** Average total cell number in control (blue bars) or *Wwc2*-specific (green bars) siRNA microinjected embryos
809 indicated developmental stages (number of embryos in each group is indicated). Errors represent s.e.m. and 2-tailed
810 student t-test derived statistical significance between control and *Wwc2* KD groups indicated (** p<0.005).
811 Supplementary tables ST3-ST8 summarise statistical analysis and individual embryo data. Note, additional data
812 describing frequencies of observable cell morphological/division defects, obtained from this same dataset are
813 presented in Fig. 3.

814

815 **Figure 3: Global *Wwc2* KD mediated cell numbers deficits are associated with defective cell division**
816 **morphologies. a)** Schematic of experimental design; 2-cell stage embryos microinjected with control or *Wwc2*-
817 specific siRNA, cultured to indicated developmental stages, fixed and assayed for total cell number or the incidence
818 of abnormal cell morphology indicative of defective cell division (determined by DAPI and rhodamine conjugated
819 phalloidin staining - note, data derived from same experiments as those described in Fig. 2). **b)** Exemplar confocal

820 micrograph z-sections of *Wwc2*-specific siRNA microinjected embryos at the 32-cell stage, illustrating three distinct
821 phenotypic morphological defect categories observed; i. abnormal nuclear morphology (including chromatin mid-
822 body association, highlighted by yellow arrows - left), ii. cytokinesis defects defined by two nuclei per cell
823 (highlighted by blue arrow -centre), iii. presence of multiple (*i.e.* >3, highlighted by pink arrows) nuclei and/or
824 micronuclei per cell (right) and iv. composite of categorised defects highlighted by colour coded arrows in a single
825 embryo confocal z-section projection (green boarder). DAPI (white) and cortical F-actin (red); scale bar = 20 μm. **c)**
826 Frequencies of each observed category of phenotypic/ morphological defect (*i.e.* micronuclei; blue, abnormal nuclei;
827 yellow and failed cytokinesis; green) or a combination of at least two or more (red) in control siRNA (left) and *Wwc2*-
828 specific siRNA (right) microinjected embryos, at indicated developmental stages (numbers of embryos in each group
829 highlighted); data demonstrate defect incidence per embryo (in at least one constituent blastomere – upper row of
830 charts) or on a per assayed cell basis (lower row of charts). Supplementary tables ST3-ST8 summarise statistical
831 analysis and individual embryo data in each experimental group.
832
833 **Figure 4: *Wwc2* mRNA is required for mouse oocyte meiotic maturation. a)** Published microarray (Wang et al.,
834 2004, blue line) and generated Q-RT-PCR (bar charts) normalised *Wwc2* mRNA expression in germinal vesicle and
835 metaphase II arrested oocytes (GV and MII) and fertilised zygotes (Tbp normalised expression, relative to GV stage).
836 Note, microarray data derived from oligo-dT primed reverse transcription and Q-RT-PCR from both oligo-dT (black
837 bars) and random hexamer priming (red bars); error bars represent s.e.m. and n=3. **b)** Experimental schema of *Wwc2*
838 KD in GV oocytes by microinjected *Wwc2* siRNA (plus control siRNA and non-microinjected controls), 18 hour
839 incubation in IMBX containing media (prevents GVBD), 16 hour *in vitro* oocyte maturation (IVM – minus IMBX)
840 and confocal microscopy or Q-RT-PCR analysis; co-microinjected RDBs used as injection control marker. **c)** Q-RT-
841 PCR data of normalised (against *Tbp*) *Wwc2* mRNA levels in control and *Wwc2* siRNA microinjected GV oocytes
842 after IVM to MII stage (error bars represent s.e.m., n=3 and ** denotes p<0.005 in 2-tailed student t-test). **d)** Charts
843 (left) detailing successful IVM frequencies of control non-microinjected (Non-Inj), microinjected control siRNA
844 (Con. siRNA) and microinjected *Wwc2* siRNA GV oocytes, to the MII stage or preceding phenotypic stages. **d')**
845 examples of successfully matured MII oocytes (note, extruded first polar body/PB1) and quantified categorised
846 phenotypes are shown as confocal z-section micrographs (right – α-Tubulin in green and DAPI DNA pseudo-
847 coloured red; scale bar = 20 μm). Supplementary tables ST14 summarise statistical analysis and individual oocyte
848 data used to generate the figure.
849
850 **Figure 5: *Wwc2* KD induced oocyte IVM phenotypes are associated with failed Aurora-A (AURKA)**
851 **phosphorylation/activation _(both rescuable by co-microinjection of siRNA resistant *HA-Wwc2* mRNA). a)**
852 Experimental schema of GV oocyte microinjection conditions; *i.e. Wwc2* siRNA or control siRNA alone or *Wwc2*
853 siRNA + *HA-Wwc2* (siRNA resistant) mRNA (*i.e.* 'rescue'), co-microinjected with RDBs (for western blot analysis)
854 or RFP-H2B mRNA (IF – fluorescent marker). Microinjected (plus non-microinjected control) oocytes incubated in
855 IMBX containing media (18 hours - to prevent GVBD), subject to IVM (max. 16 hours – media minus IMBX) and
856 processed for western blotting and IF at designated oocyte maturation time-points (assaying phospho-Aurora/ p-
857 AURKA levels) or assayed for developmental progression/*Wwc2* KD induced phenotypes. **b)** Western blots of
858 activated p-AURKA levels (plus GAPDH housekeeping control), at indicated stages of oocyte maturation (note, GV;

859 +0 hours relative to IMBX washout, metaphase of meiosis I/ MI; +7 hours and MII; +16 hours), in either control or
860 *Wwc2* siRNA microinjected, or non-microinjected conditions. **c)** Exemplar single confocal z-section IF micrographs
861 of control (left) or *Wwc2* siRNA (right) IVM cultured microinjected oocytes at the MII equivalent stage (16 hours
862 post-IBMX) stained for p-AURKA (green) and α-TUBULIN (white) and labelled with RFP-H2B chromatin reporter
863 (red); insets show zoomed region of meiotic spindle. Note, *Wwc2* siRNA microinjection group example image is
864 over-saturated compared to control (to illustrate lack of spindle associated pAURKA – cortical signal is auto-
865 fluorescence); PB1 (control siRNA) denotes extruded first polar body and the scale bars represents 20 μm. **d)** Chart
866 detailing IVM rates of control siRNA, *Wwc2* siRNA and *Wwc2* siRNA + *HA-Wwc2* mRNA (rescue) microinjected
867 oocytes at staged time-points post IBMX removal; as described by percentage of oocytes at any of stated IVM stages
868 or categorised phenotypes (typically associated with *Wwc2* KD – see Fig. 4); number of oocytes in each experimental
869 condition at each assayed IVM stage is indicated. **e)** Western blot of activated p-AURKA levels (plus GAPDH
870 housekeeping control) at MII equivalent stage (16 hours post-IVM), in control siRNA, *Wwc2* siRNA or *Wwc2* siRNA
871 + *HA-Wwc2* mRNA microinjected (rescue) oocytes. Supplementary tables S16-19 summarise statistical analysis and
872 individual oocyte data used to generate the figure.
873
874 **Figure 6: Outer trophectoderm (TE) versus ICM formation in clonal *Wwc2* gene KD at early blastocyst stage.**
875 **a)** Experimental strategy for *Wwc2* expression KD in marked clones (representing 50% of embryo) by co-
876 microinjection (in one blastomere of 2-cell stage embryos) of *Wwc2* siRNA and GAP43-GFP mRNA (stable plasma
877 membrane fluorescent injection clone marker – Inj.) and IF based assay of clonal contribution (Inj vs. Non) to CDX2
878 (TE marker) positive or negative cells, plus outer and inner-cell embryo populations at 32-cell stage (versus control
879 siRNA microinjections). **b)** Exemplar confocal z-section micrographs of IF stained blastocysts (individual greyscale
880 channels plus merged image; CDX2 is red) from control and *Wwc2* siRNA microinjected groups. Note, white arrows
881 and yellow arrow head denote DAPI stained micronuclei and a bi-nucleated cell, respectively, uniquely found in
882 *Wwc2* siRNA microinjected clones. Blue and white asterisks denote respective low level (compared to non-injected
883 clone) or undetectable outer-cell CDX2 protein expression in *Wwc2* KD clones. The number of embryos in each
884 group is provided; scale bar equals 20μm. **c)** Left - pie charts detailing average distribution of CDX2 protein
885 expression (positive or negative) between control and *Wwc2* siRNA groups, in both outer or ICM cells (note, pie
886 chart areas for each spatial population are scaled to that summarising the whole embryo; similarly, pie chart area
887 describing the whole embryo in the *Wwc2* siRNA condition is scaled to that in the control siRNA group). Right -
888 average clonal contribution (Inj vs. Non) of outer and ICM cells in control (blue bars) and *Wwc2* siRNA (green bars)
889 microinjected embryos, irrespective of CDX2 expression. **d)** As in c) only describing clonal contribution of CDX2
890 expressing (or not) cells to outer and ICM populations, as a fraction of the total sub-population size (left - pie charts)
891 or in raw average cell number (right – bar charts) In panel c) and d) charts, errors represent s.e.m. and 2-tailed student
892 t-test derived statistical significance between control and *Wwc2* KD groups (asterisks), or clones (Inj. vs Non) within
893 a group (double crosses) are highlighted with statistical confidence intervals of $p<0.05$ and $p<0.005$, as denoted by
894 one or two significance markers, respectively. Supplementary tables ST20 summarise statistical analysis and
895 individual embryo data.
896

897 **Figure 7: Overall cell lineage formation after clonal *Wwc2* gene KD at the late blastocyst stage. a)** Experimental
898 strategy for *Wwc2* expression KD in marked clones (representing 50% of the embryo) by co-microinjection (in one
899 blastomere of 2-cell stage embryos) of *Wwc2* siRNA and GAP43-GFP mRNA (stable plasma membrane fluorescent
900 injection clone marker lineage marker – Inj.) and an IF based assay of clonal contribution (Inj vs. Non) to blastocyst
901 protein lineage marker expressing cells (TE; CDX2, PrE; GATA4, EPI; NANOG or SOX2; assayed in combination
902 – see below), plus outer and inner-cell embryo populations, at the late blastocyst stage (versus control siRNA
903 microinjections). **b)** Average number of apoptotic cells in control and *Wwc2* siRNA microinjected embryo groups
904 (averaged across all IF regimes – see below) in outer and inner cell populations and clones (Inj. vs. Non); errors
905 represent s.e.m. and 2-tailed student t-test derived statistical significance between control and *Wwc2* KD groups
906 (asterisks) or clones (Inj. vs Non) within a group (double crosses) highlighted with statistical confidence intervals of
907 $p<0.05$ and $p<0.005$ (denoted by one or two significance markers, respectively). **c)** Exemplar confocal z-section
908 micrographs of IF stained blastocysts (individual greyscale channels plus merged images, in which assayed
909 combinations of cell lineage markers are respectively coloured green and red; CDX2 & NANOG, GATA4 & NANOG
910 and GATA4 and SOX2) from control and *Wwc2* siRNA microinjected groups. Within the *Wwc2* siRNA microinjected
911 clone, yellow arrows denote apoptotic cell remnants, blue arrows interphase ICM cells that neither express GATA4
912 or NANOG, the yellow arrow head a bi-nucleated cell whereas blue or white asterisks highlight outer-cells with basal
913 or undetectable CDX2 expression, respectively. The number of assayed embryos in each control (Con) and *Wwc2*
914 siRNA (KD) microinjection group is provided; scale bar equals 20µm. **d)** Pie charts detailing, (left of panel), average
915 distribution of detectable CDX2 and NANOG protein expression (positive or negative) between control and *Wwc2*
916 siRNA groups, in both outer or ICM cells (note, pie chart areas for each spatial population are scaled to that
917 summarising the whole embryo; similarly the pie chart area describing the whole embryo in the *Wwc2* siRNA
918 condition is scaled to that in the control siRNA group). Central and right panels, contain pie charts describing clonal
919 contribution of CDX2 and NANOG expressing (or not) cells to outer and ICM populations, as a fraction of the total
920 sub-population size. **e)** As in d) only assaying NANOG (EPI) and GATA4 (PrE) expression. **f)** As in d) only assaying
921 SOX2 (EPI) and GATA4 (PrE) expression. Note, supplementary figure S8 details the same data in raw average cell
922 number format (*i.e.* as presented in Fig. 6d - bar charts on right) and supplementary tables ST21-ST23 summarise
923 statistical analysis and individual embryo data.
924
925 **Figure 8: Expression of siRNA resistant *HA-Wwc2* mRNA rescues *Wwc2* siRNA cell number/division**
926 **phenotypes. a)** Experimental strategy for potential phenotypic rescue of clonal *Wwc2* KD by comparing co-
927 microinjection (in one blastomere of 2-cell stage embryos) of GAP43-GFP mRNA (stable plasma membrane
928 fluorescent injection marker – Inj.; to distinguish from the non-microinjected clone – Non inj.) with control siRNA,
929 *Wwc2* siRNA or *Wwc2* siRNA + recombinant *HA-Wwc2* mRNA (containing N-terminal HA-epitope tag and point
930 mutants conferring siRNA resistance – see supplementary figure S5) and assaying total, outer and inner-cell number
931 at the 32-cell and late blastocyst (>64-cell) stages. **b)** Average clonal contribution (Inj vs. Non) of outer and ICM
932 cells in control siRNA (blue bars), *Wwc2* siRNA (green bars) and *Wwc2* siRNA + *HA-Wwc2* mRNA (rescue – orange
933 bars) microinjected embryos; errors represent s.e.m. and 2-tailed student t-test derived statistical significance between
934 the experimental groups (asterisks), or clones (Inj. vs Non inj.) within a group (double crosses) highlighted with
935 statistical confidence intervals of $p<0.05$ and $p<0.005$ (denoted by one or two significance markers, respectively).

936 The number of embryos in each experimental group is provided. **c)** Pie charts detailing overall and clonal distribution
937 of constituent embryo cells between outer and inner-cell populations, plus the incidence of abnormal nuclear
938 morphology (as defined in Fig. 3), in each of the three indicated experimental groups, at the 32-cell (left) and late
939 blastocyst (right) stages. Note, areas of all individual pie chart categories are normalised against those describing the
940 appropriate criteria in the control siRNA condition. **d)** Exemplar confocal z-section micrographs of 32-cell and late
941 blastocyst stage embryos, derived from the indicated microinjection groups, IF stained to detect HA-epitope tag
942 expression (individual greyscale channels plus merged images - anti-HA channel is red and the DAPI cyan). Within
943 microinjected clones of *Wwc2* siRNA treated groups, white or red asterisks respectively denote characteristic
944 abnormal mitotic or apoptotic cell remnants, whilst in the microinjected clone of *Wwc2* siRNA + *HA-Wwc2* rescue
945 group, white arrows indicate anti-HA epitope tag signal associated with mid-bodies, particular characteristic, in 32-
946 cell stage embryos (see also indicated zoomed images); scale bar equals 20μm. Supplementary tables ST24 & ST25
947 summarise statistical analysis and individual embryo data used to generate the figure.

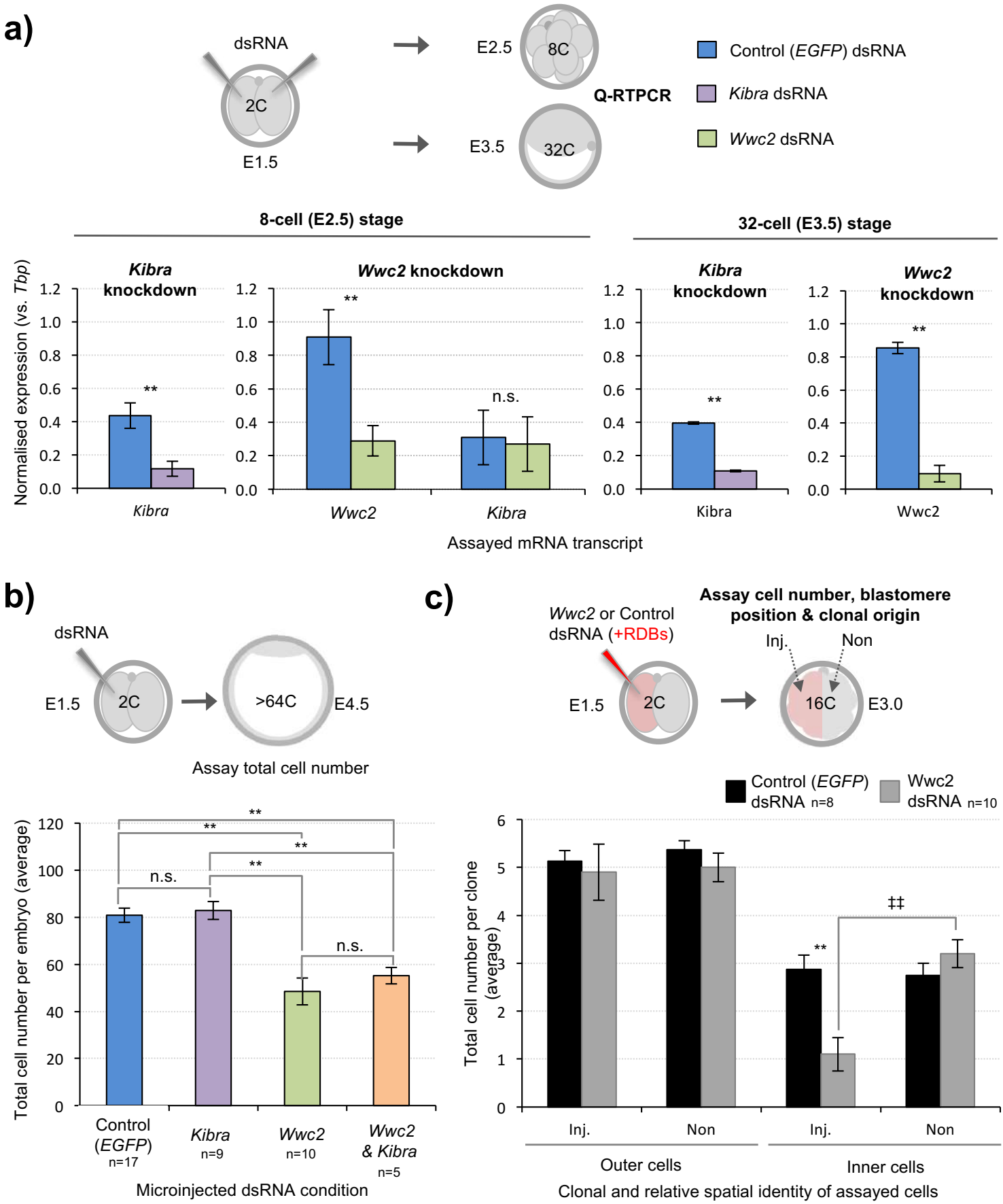
a)
dsRNA
2C
E1.5
E2.5
8C
E3.5
32C
Q-RTPCR
Control (EGFP) dsRNA
Kibra dsRNA
Wwc2 dsRNA
8-cell (E2.5) stage
32-cell (E3.5) stage
Kibra knockdown
Wwc2 knockdown
Normalised expression (vs. Tbp)
Kibra
Wwc2
Kibra
Kibra
Wwc2
Assayed mRNA transcript
b)
dsRNA
E1.5
2C
>64C
E4.5
Assay total cell number
Total cell number per embryo (average)
Control (EGFP) n=17
Kibra n=9
Wwc2 n=10
Wwc2 & Kibra n=5
Microinjected dsRNA condition
c)
Wwc2 or Control dsRNA (+RDBs)
Assay cell number, blastomere position & clonal origin
Inj.
Non
E1.5
2C
16C
E3.0
Control (EGFP) dsRNA n=8
Wwc2 dsRNA n=10
Total cell number per clone (average)
Inj.
Non
Inj.
Non
Outer cells
Inner cells
Clonal and relative spatial identity of assayed cells

Fig. 1

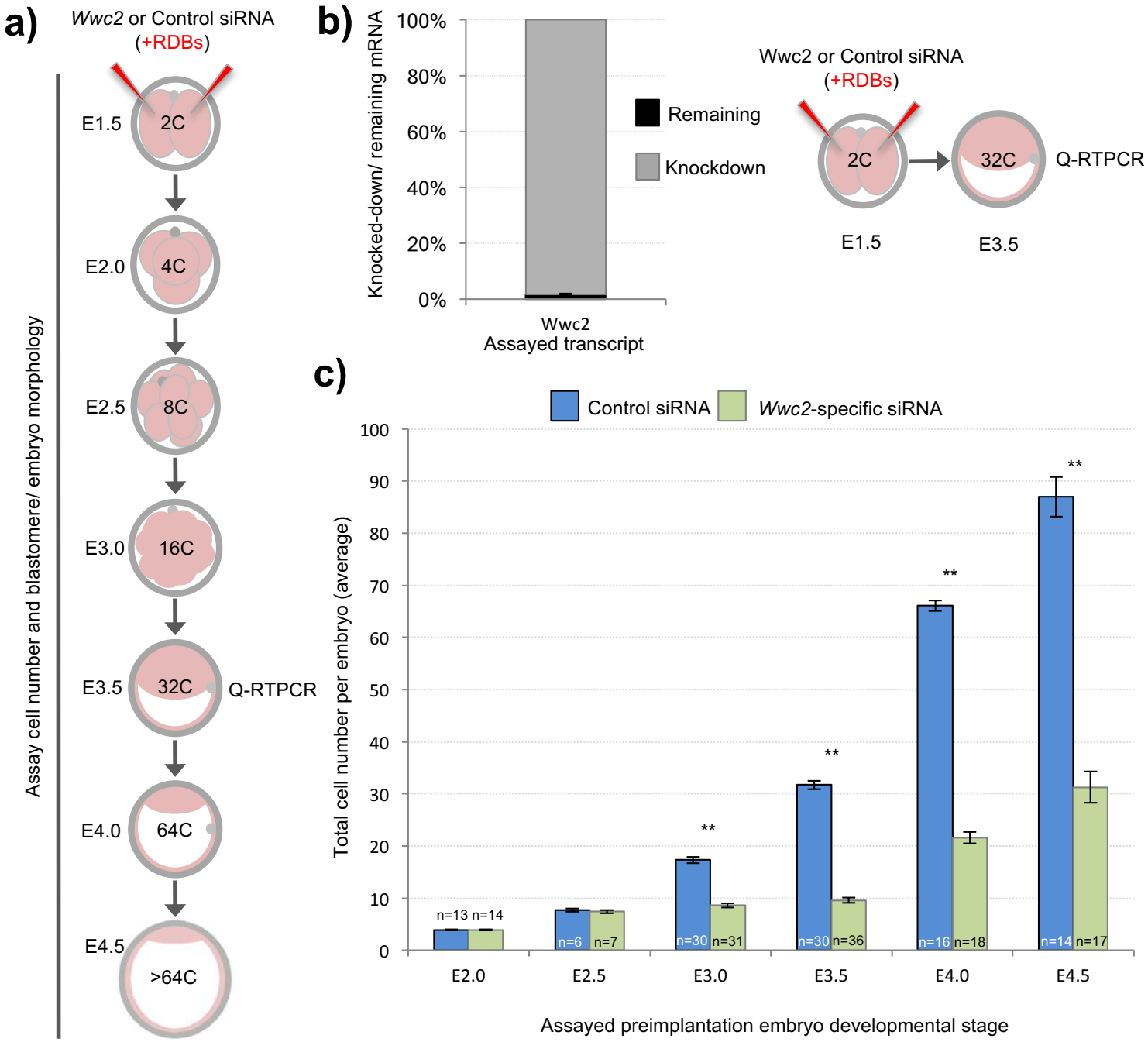
a)
Wwc2 or Control siRNA
(+RDBs)
E1.5
2C
E2.0
4C
E2.5
8C
E3.0
16C
E3.5
32C
Q-RTPCR
E4.0
64C
E4.5
>64C
Assay cell number and blastomere/ embryo morphology
b)
Knocked-down/ remaining mRNA
100%
80%
60%
40%
20%
0%
Remaining
Knockdown
Wwc2
Assayed transcript
Wwc2 or Control siRNA
(+RDBs)
2C
32C
Q-RTPCR
E1.5
E3.5
c)
Control siRNA
Wwc2-specific siRNA
Total cell number per embryo (average)
100
90
80
70
60
50
40
30
20
10
0
**
n=13 n=14
n=6
n=7
n=30
n=31
n=30
n=36
n=16
n=18
n=14
n=17
E2.0
E2.5
E3.0
E3.5
E4.0
E4.5
Assayed preimplantation embryo developmental stage

Fig. 2

Fig. 3

a)

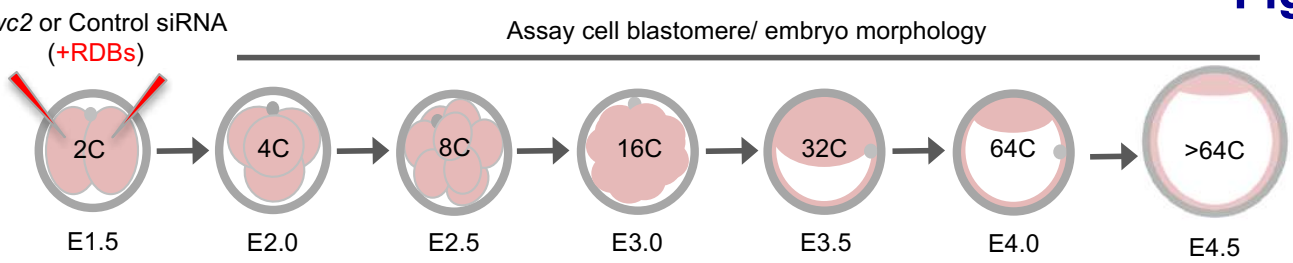

b)

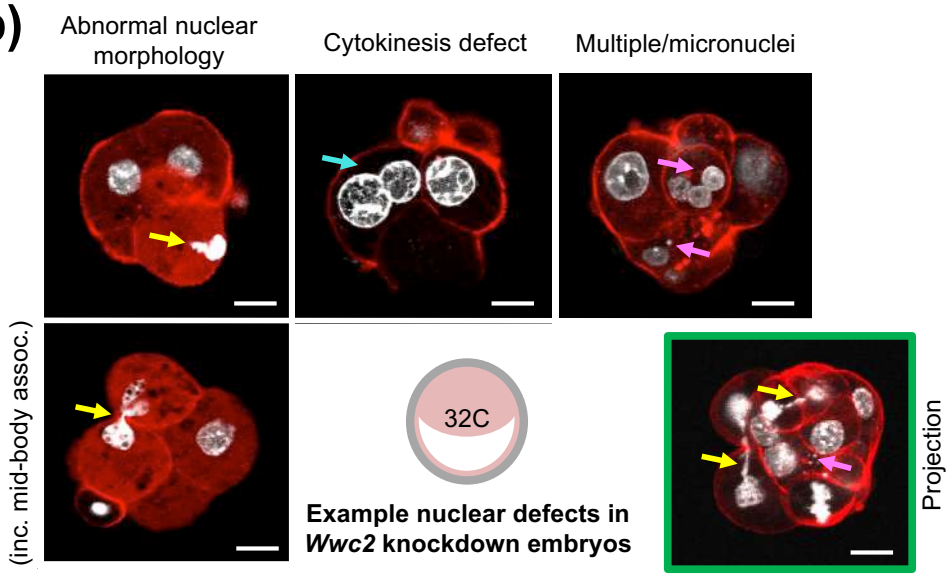

c)

Phenotype		
Presence of multiple/ micronuclei	Observed	
	Unobserved	
Abnormal nuclear morphology	Observed	
	Unobserved	
Cytokinesis defect	Observed	
	Unobserved	
Amalgamated phenotypes	Observed	
	Unobserved	

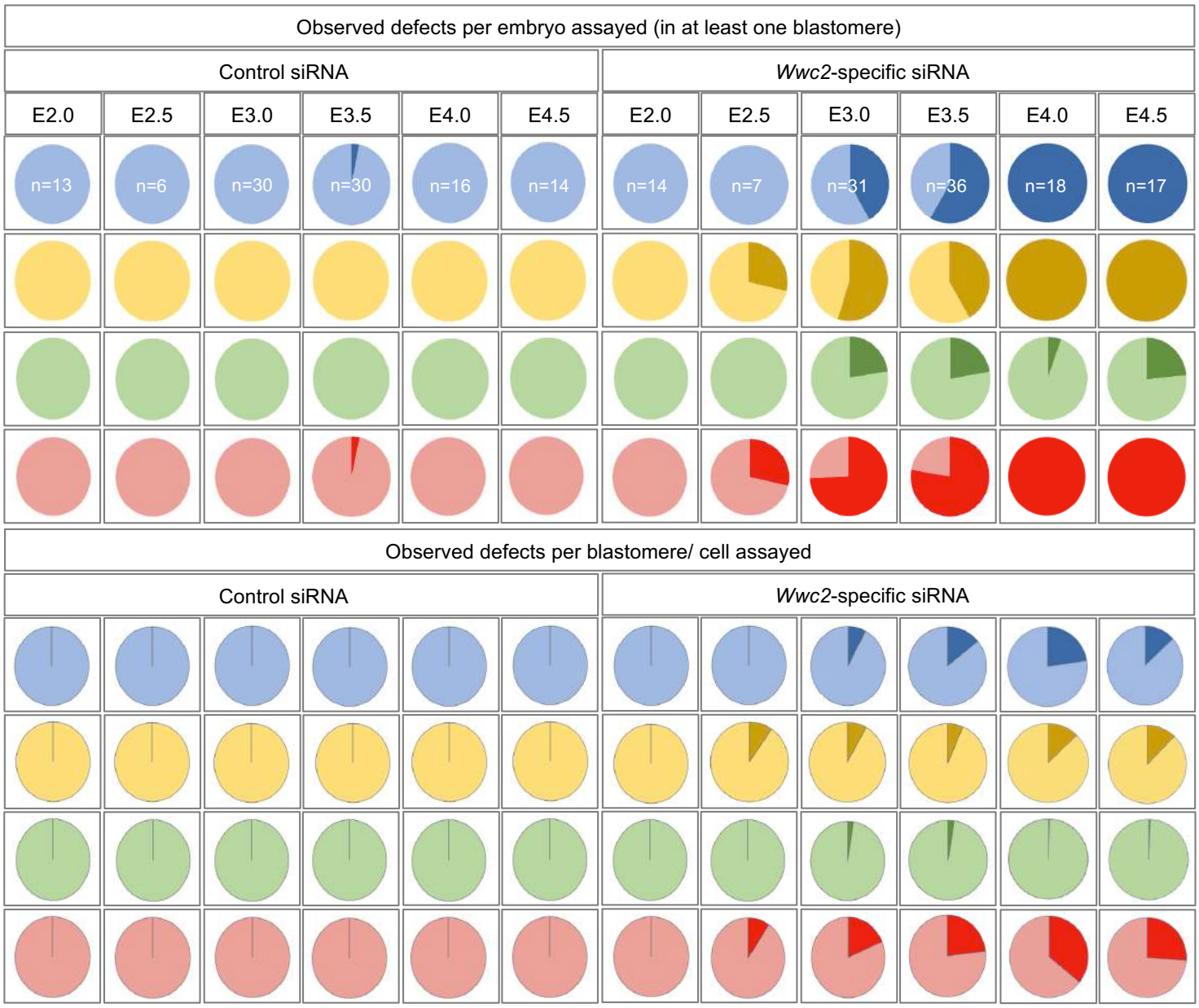

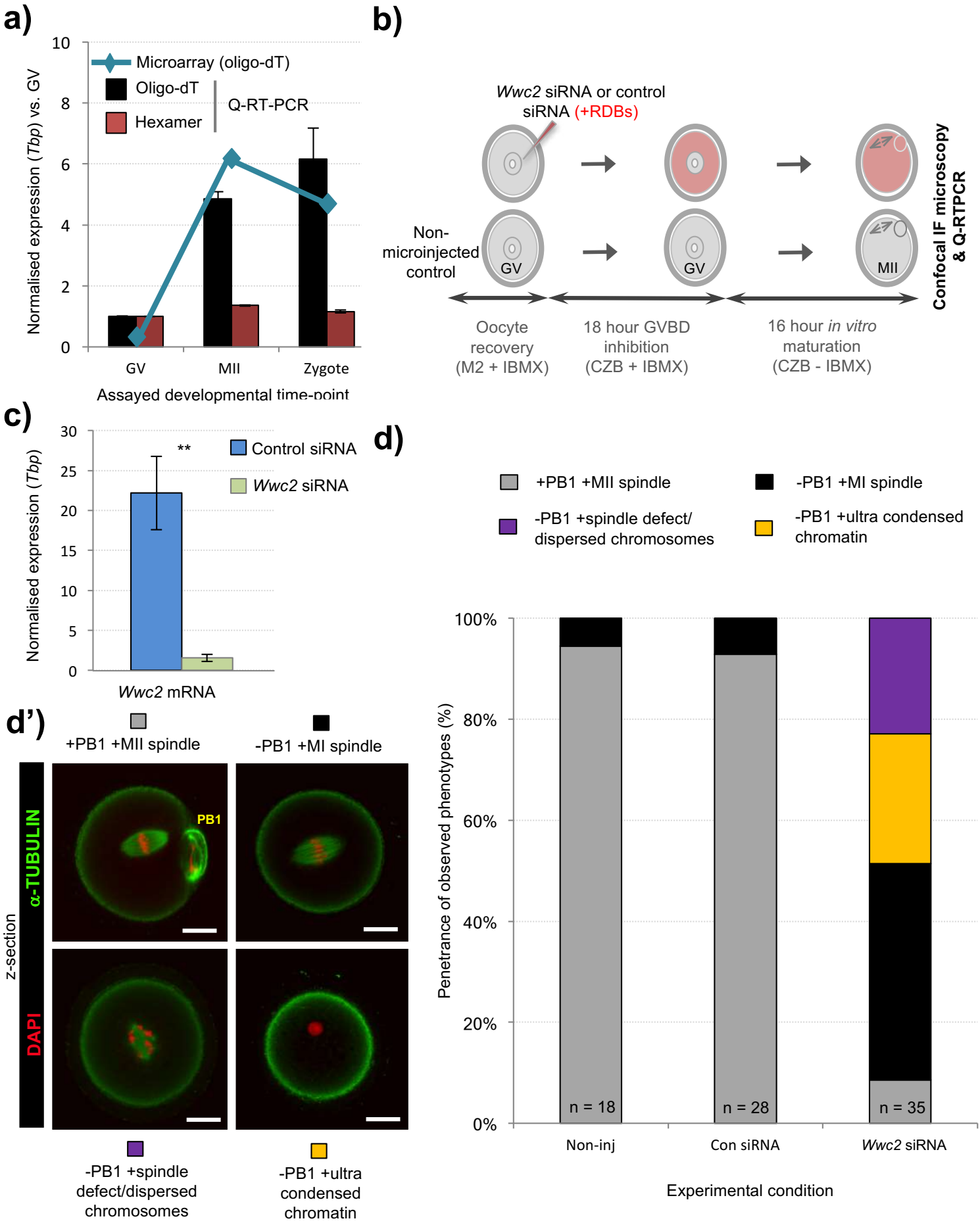
a)
Microarray (oligo-dT)
Oligo-dT
Hexamer
Q-RT-PCR
Normalised expression (Tbp) vs. GV
GV
MII
Zygote
Assayed developmental time-point
b)
Wwc2 siRNA or control siRNA (+RDBs)
Non-microinjected control
GV
GV
MII
Confocal IF microscopy & Q-RTPCR
Oocyte recovery (M2 + IBMX)
18 hour GVBD inhibition (CZB + IBMX)
16 hour in vitro maturation (CZB - IBMX)
c)
Control siRNA
Wwc2 siRNA
**
Normalised expression (Tbp)
Wwc2 mRNA
d)
+PB1 +MII spindle
-PB1 +MI spindle
-PB1 +spindle defect/ dispersed chromosomes
-PB1 +ultra condensed chromatin
Penetrance of observed phenotypes (%)
n = 18
n = 28
n = 35
Non-inj
Con siRNA
Wwc2 siRNA
Experimental condition
d')
+PB1 +MII spindle
-PB1 +MI spindle
α-TUBULIN
DAPI
z-section
PB1
-PB1 +spindle defect/dispersed chromosomes
-PB1 +ultra condensed chromatin

Fig. 4

Fig. 5

a)

Wwc2 siRNA, control siRNA or *Wwc2* siRNA + *HA-Wwc2* (siRNA resistant) mRNA (rescue)
(+RDBs – WB or +RFP-H2B mRNA - IF)

Non-microinjected control

GV → GV → MII

Detection of p-AURKA (p-Thr288) expression/ activation

Western blotting (WB)

Immuno-fluorescence staining (IF)

Oocyte recovery (M2 + IBMX) | 18 hour GVBD inhibition (CZB + IBMX) | 16 hour *in vitro* maturation (CZB - IBMX)

b)

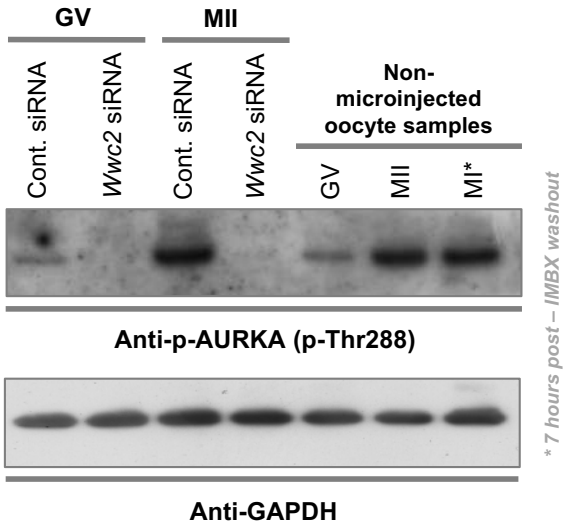

c)

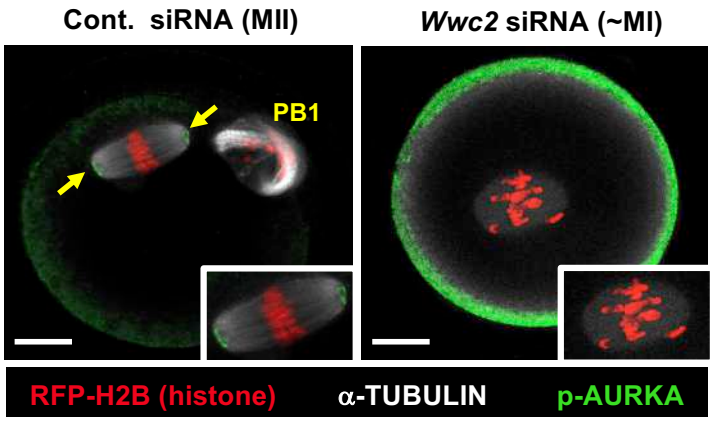

d)

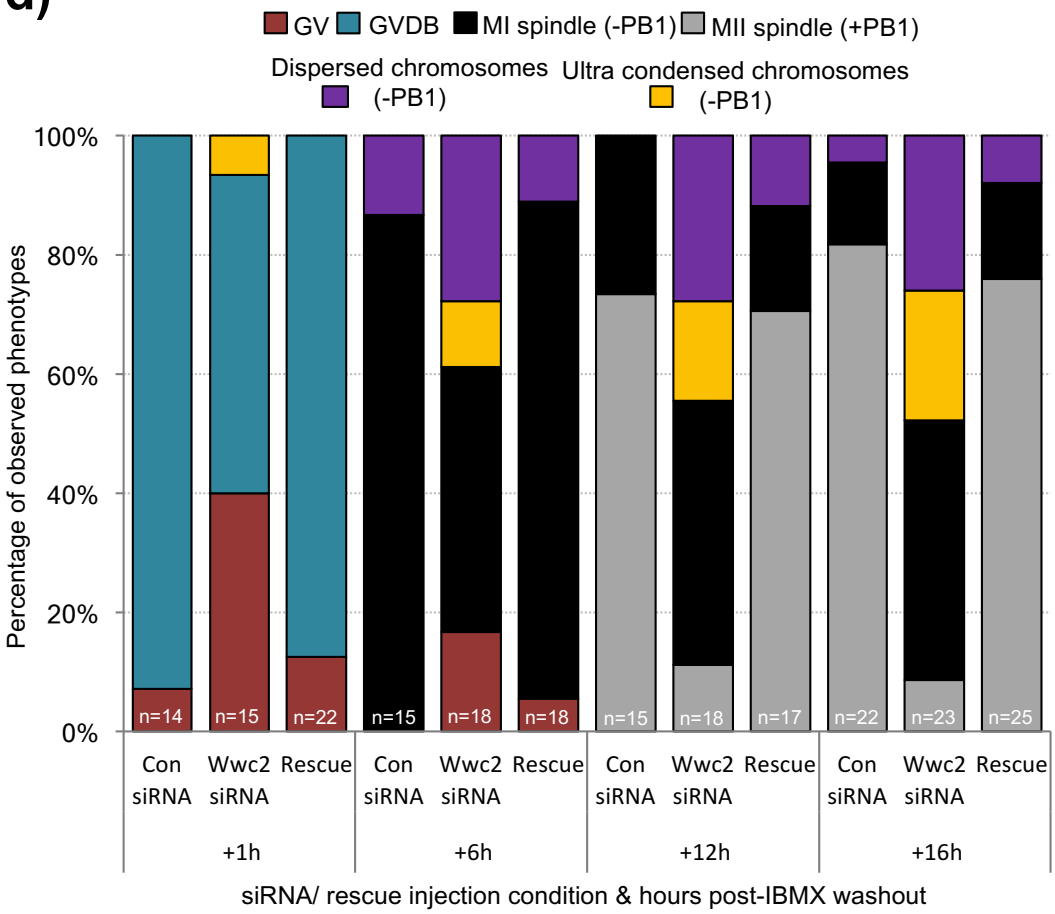

e)

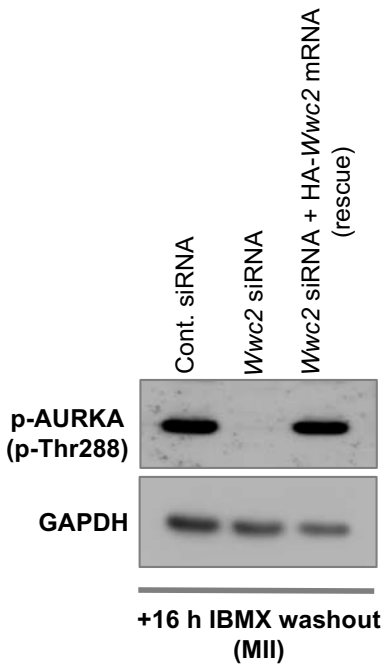

Fig. 6

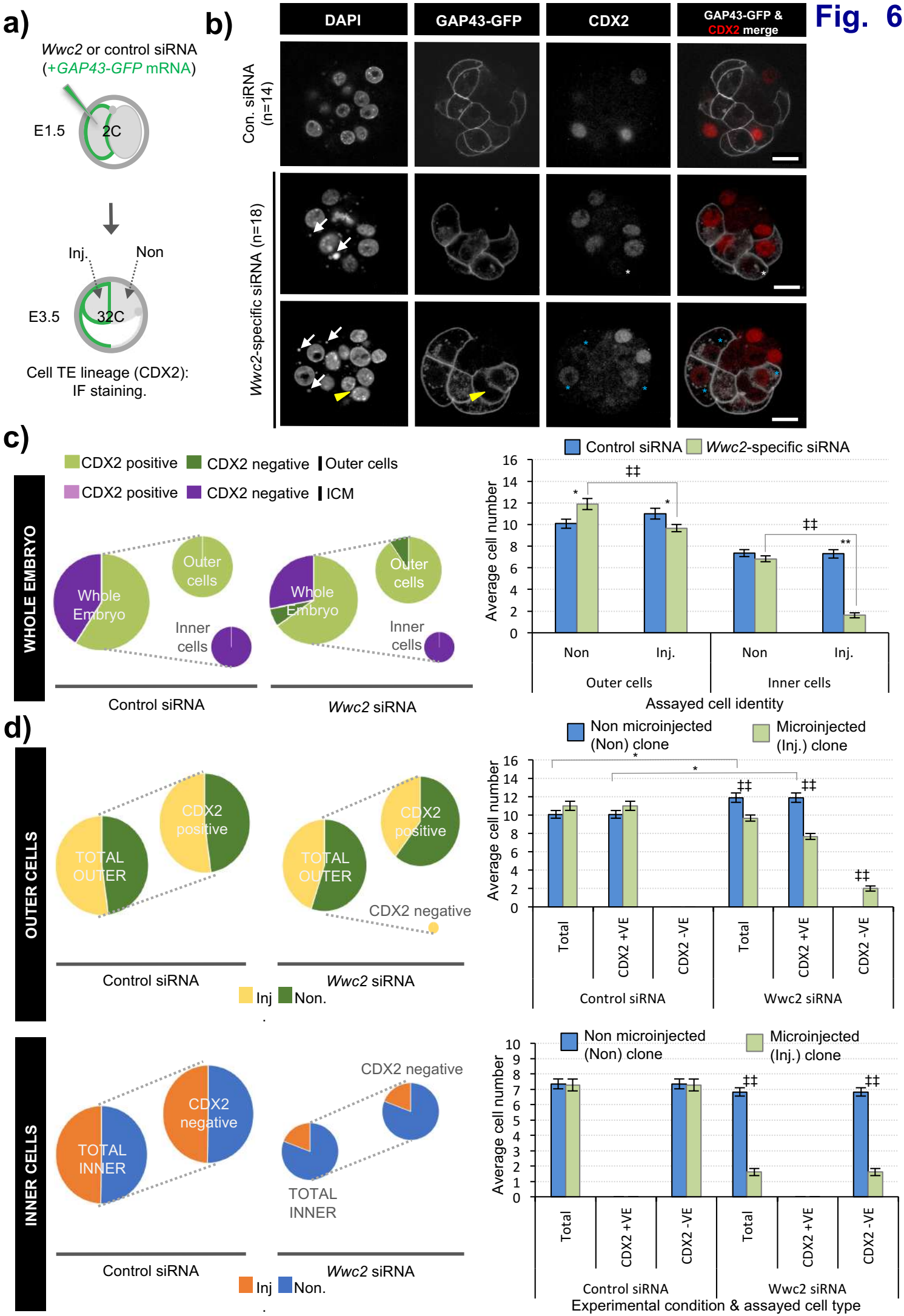
a)
Wwc2 or control siRNA
(+GAP43-GFP mRNA)
E1.5
2C
Inj.
Non
E3.5
32C
Cell TE lineage (CDX2):
IF staining.
b)
DAPI
GAP43-GFP
CDX2
GAP43-GFP & CDX2 merge
Con. siRNA (n=14)
Wwc2-specific siRNA (n=18)
c)
CDX2 positive
CDX2 negative
Outer cells
CDX2 positive
CDX2 negative
ICM
WHOLE EMBRYO
Whole Embryo
Outer cells
Inner cells
Control siRNA
Wwc2 siRNA
Control siRNA
Wwc2-specific siRNA
Average cell number
Non
Inj.
Outer cells
Inner cells
Assayed cell identity
d)
OUTER CELLS
TOTAL OUTER
CDX2 positive
CDX2 negative
Control siRNA
Wwc2 siRNA
Inj
Non.
Non microinjected (Non) clone
Microinjected (Inj.) clone
Total
CDX2 +VE
CDX2 -VE
Control siRNA
Wwc2 siRNA
INNER CELLS
TOTAL INNER
CDX2 negative
Control siRNA
Wwc2 siRNA
Inj
Non.
Experimental condition & assayed cell type

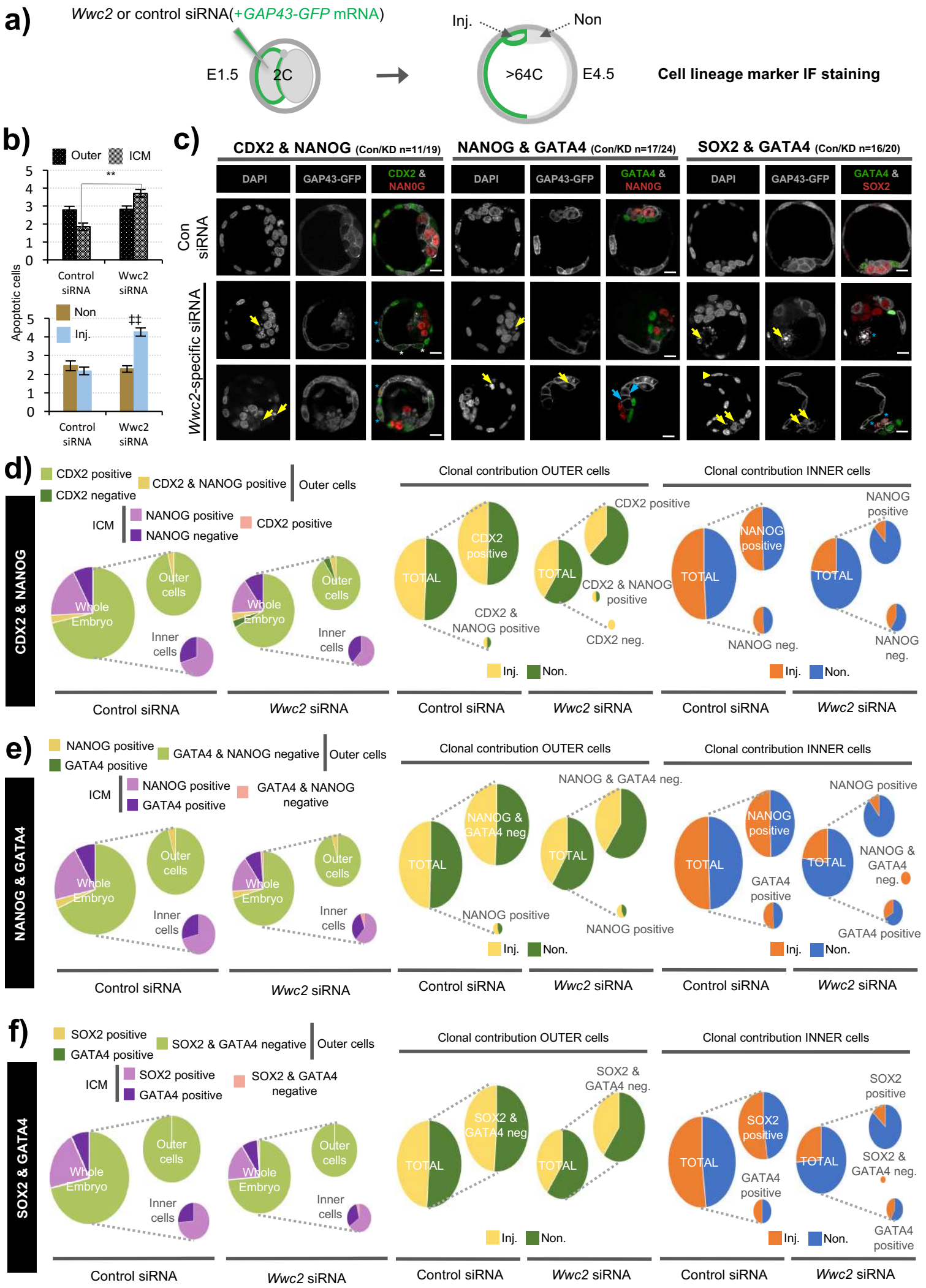
a)
Wwc2 or control siRNA(+GAP43-GFP mRNA)
E1.5
2C
Inj.
Non
>64C
E4.5
Cell lineage marker IF staining
b)
Outer
ICM
Apoptotic cells
Control siRNA
Wwc2 siRNA
Non
Inj.
c)
CDX2 & NANOG (Con/KD n=11/19)
NANOG & GATA4 (Con/KD n=17/24)
SOX2 & GATA4 (Con/KD n=16/20)
DAPI
GAP43-GFP
CDX2 & NANOG
GATA4 & NANOG
GATA4 & SOX2
Con siRNA
Wwc2-specific siRNA
d)
CDX2 positive
CDX2 & NANOG positive
Outer cells
CDX2 negative
ICM
NANOG positive
NANOG negative
CDX2 positive
Clonal contribution OUTER cells
Clonal contribution INNER cells
Whole Embryo
Outer cells
Inner cells
TOTAL
CDX2 positive
CDX2 & NANOG positive
CDX2 neg.
NANOG positive
NANOG neg.
Inj.
Non.
Control siRNA
Wwc2 siRNA
CDX2 & NANOG
e)
NANOG positive
GATA4 & NANOG negative
GATA4 positive
GATA4 & NANOG negative
NANOG & GATA4 neg.
GATA4 positive
NANOG & GATA4
f)
SOX2 positive
SOX2 & GATA4 negative
SOX2 & GATA4 neg.
SOX2 & GATA4
Fig. 7

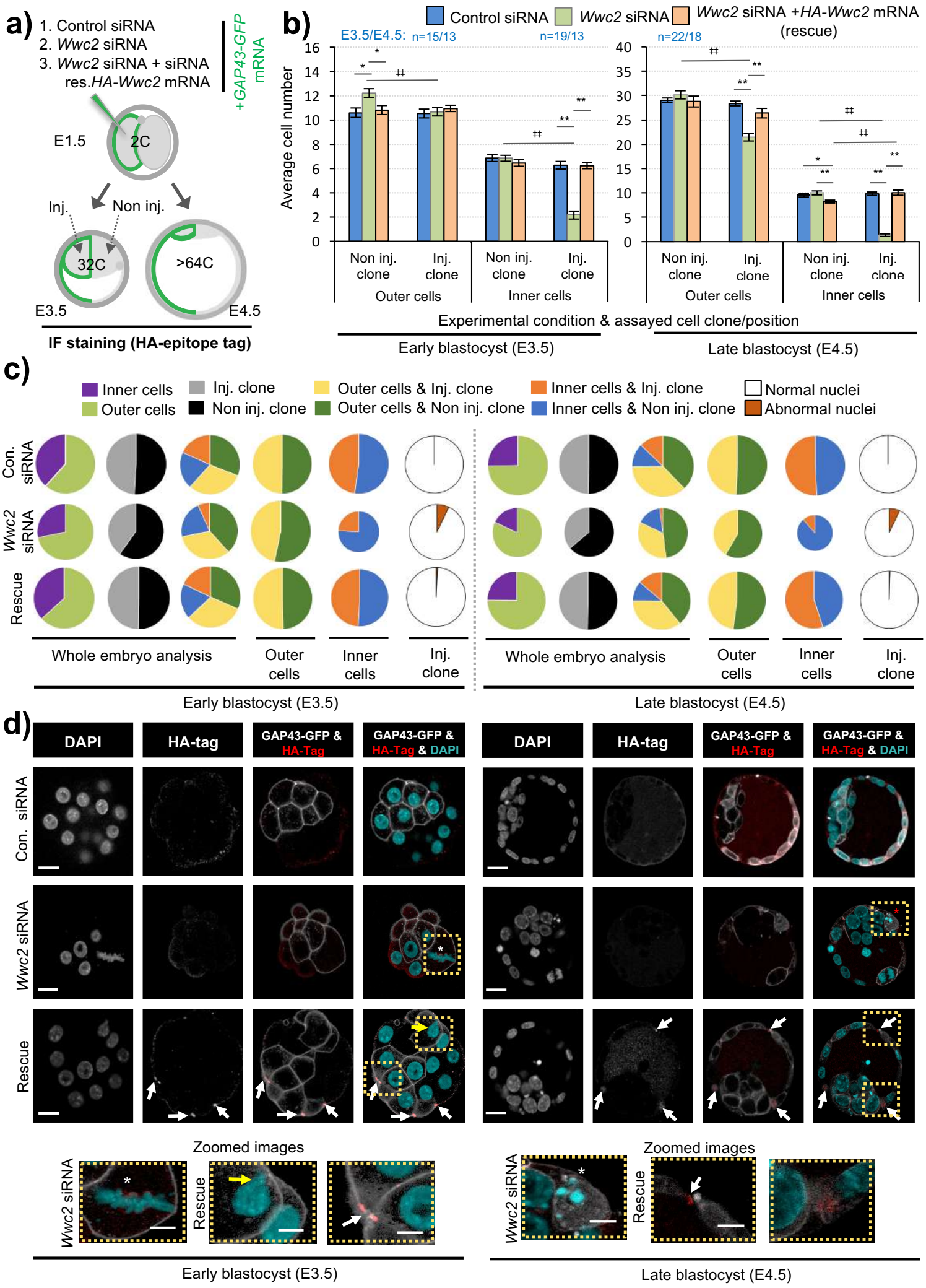
a)
1. Control siRNA
2. Wwc2 siRNA
3. Wwc2 siRNA + siRNA res.HA-Wwc2 mRNA
+GAP43-GFP mRNA
E1.5
2C
Inj.
Non inj.
32C
>64C
E3.5
E4.5
IF staining (HA-epitope tag)
b)
Control siRNA
Wwc2 siRNA
Wwc2 siRNA +HA-Wwc2 mRNA (rescue)
E3.5/E4.5: n=15/13
n=19/13
n=22/18
Average cell number
Non inj. clone
Inj. clone
Outer cells
Inner cells
Experimental condition & assayed cell clone/position
Early blastocyst (E3.5)
Late blastocyst (E4.5)
c)
Inner cells
Outer cells
Inj. clone
Non inj. clone
Outer cells & Inj. clone
Outer cells & Non inj. clone
Inner cells & Inj. clone
Inner cells & Non inj. clone
Normal nuclei
Abnormal nuclei
Con. siRNA
Wwc2 siRNA
Rescue
Whole embryo analysis
Outer cells
Inner cells
Inj. clone
Early blastocyst (E3.5)
Late blastocyst (E4.5)
d)
DAPI
HA-tag
GAP43-GFP & HA-Tag
GAP43-GFP & HA-Tag & DAPI
Con. siRNA
Wwc2 siRNA
Rescue
Zoomed images
Wwc2 siRNA
Rescue
Early blastocyst (E3.5)
Late blastocyst (E4.5)

Fig. 8